CERN SPSC 2007-020
SPSC-M-756
June 18, 2007

Status Report and Beam Time Request for Experiment AD-4 Biological Effectiveness of Antiproton Annihilation

Michael Holzscheiter[1], Jan Alsner[2], Niels Bassler[2,3], Gerd Beyer[4], John DeMarco[5], Michael Doser[6], Dragan Hajdukovic[7], Oliver Hartley[4], Kei Iwamoto[5], Oliver Jäkel[3], Helge Knudsen[8], Sandra Kovacevic[7], Bill McBride[5], Søren Pape Møller[8], Jens Overgaard[2], Jørgen Petersen[2], Osman Ratib[4], Timothy Solberg[9], Ulrik Uggerhøj[8], Sanja Vranjes[10], and Brad Wouters[11]

[1] University of New Mexico
[2]Aarhus University Hospital
[3] Deutsches Krebsforschungszentrum
[4] Geneva University Hospital
[5] University of California at Los Angeles
[6] CERN
[7] University of Montenegro
[8] Aarhus University
[9] University of Nebraska Medical Center
[11]University of Maastricht
[10] Vinca Institute of Nuclear Sciences

Summary

A first round of experiments conducted in 2003 and 2004 at CERN and at TRIUMF have shown a significant enhancement of the biological effective dose ratio (BEDR) for antiprotons compared to protons. The experimental methods and analysis as well as the definition of terms used are described in the 2006 publication in Radiotherapy & Oncology (see appendix B). In 2006 the AD-4 collaboration conducted a set of experiments at higher beam energy and therefore deeper penetration into the target. We also used for the first time a spread-out Bragg peak (SOBP), as is standard in regular treatment situations. Early 2007 we performed a set of irradiations using the same methods and materials at GSI with carbon ions giving the same penetration depth and the same SOBP as the antiprotons at CERN. Due to problems with the a priori estimate of dose in the case of antiprotons, a number of data points were rendered unusable and the preliminary results presented in this report cannot be considered conclusive. This leads us to the request for another period of beam time in which we will increase the efforts on dosimetry and beam development prior to the biological measurements. The data taken at GSI used a beam of clinical quality with excellent absolute dosimetry available and these data are in excellent agreement with other studies on biological effects of carbon ion.

Parallel to the biological measurements with antiprotons we performed several experiments aimed at improving the dosimetry of the antiproton beam. Two problems needed to be overcome. Not only is the response to high LET radiation for most dosimeters not well understood, but in addition, the pulsed time structure of the beam makes the instantaneous dose rate too high for most standard dosimeters to handle. We used Alanine tablets and ionization chambers to measure the response to the antiproton beam and then compared these results to predictions using different Monte Carlo calculations. We found good agreement between the code package FLUKA and the measurements using both types of detectors and feel confident that we can estimate absolute dose within 10 to 20% in future experiments.

I. Biological Measurements:

In October 2006 we performed our first studies of cell survival using a 502 MeV/c antiproton beam from the AD. This beam energy allowed a penetration into our target of approximately 10 cm and much more closely resembled possible therapeutic situations. In addition we used a set of passive degraders to generate a spread-out Bragg peak of 10 mm depth, irradiating a volume of approximately 300 mm^3. The dose-depth profile for both antiprotons and carbon ions are shown in figure 1.

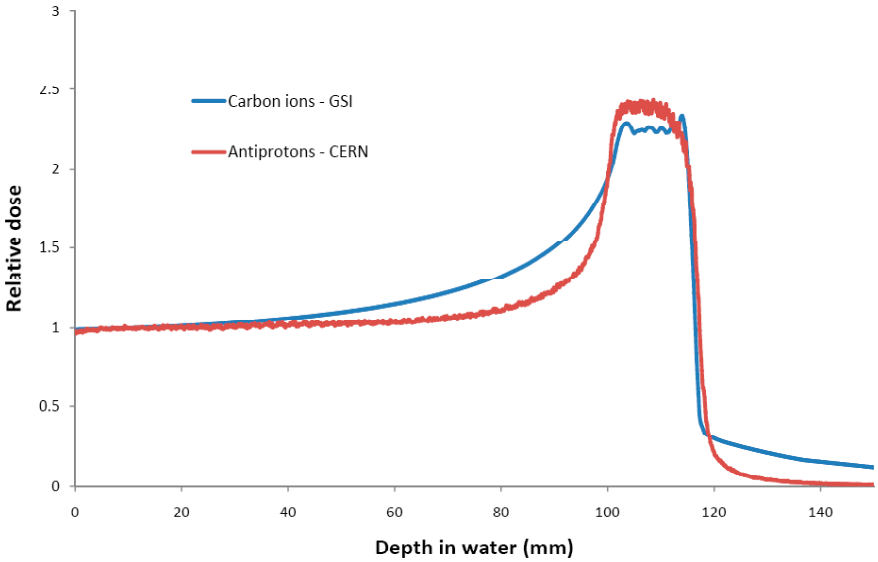

Fig. 1: Relative dose for carbon ions and antiprotons vs. depth in the target.

Within the maximum allowable time for a single set of biological measurements, dictated by the overall survival time of the cell cultures from harvesting to analyzing, we performed 4 different irradiations with nominal dose values of 0.25, 0.5, 1, and 5 Gy. Preliminary analyses of the antiproton data showed that our estimate of deposited dose was based on a faulty value of the beam diameter and that a number of data points were unusable. This was caused by the fact that we had to rely on the beam diameter value obtained from a fit to the read-out of the last wire chamber in the DEM line. Due to the course grid of this chamber and a suspected bug in the fitting software the beam diameter was overestimated by a factor of 1.7 and the dose therefore underestimated by a factor of 2.9. This error not only caused a complete overkill in the nominal 5 Gy run, but also limited us to the 4 measurements within the allowable time frame. The actual total dose delivered during this set was 20 Gy and would have allowed us to collect meaningful data for at least twice as many points below the 5 Gy value. Figure 2 below shows the raw data on cell survival vs. depth obtained in this experiment (note the sharp rise in cell kill with depth near the Bragg peak).

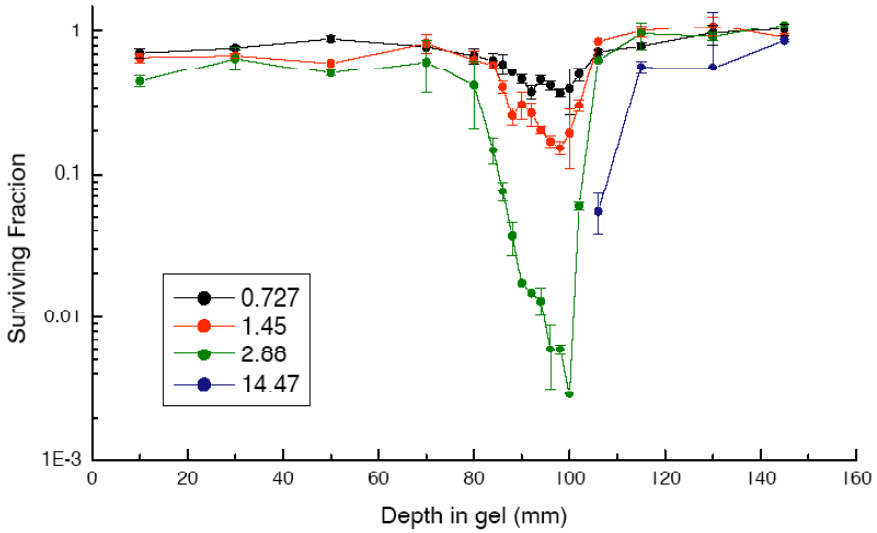

Fig. 2: Survival fraction vs. depth in the target for V79 Chinese Hamster cells irradiated with antiprotons. The dose values used as labels are estimated from FLUKA calculations using the number of antiprotons delivered and the radial beam profile obtained from radiochromic film irradiated simultaneously with the cell samples and analyzed after the run.

In early 2007 we conducted an experiment using carbon ions at GSI. Here a beam of clinical quality and absolute dosimetry is available. We performed survival measurements on 8 samples with plateau dose values between 0.3 and 4.0 Gy. Survival data vs. depth are shown in figure 3.

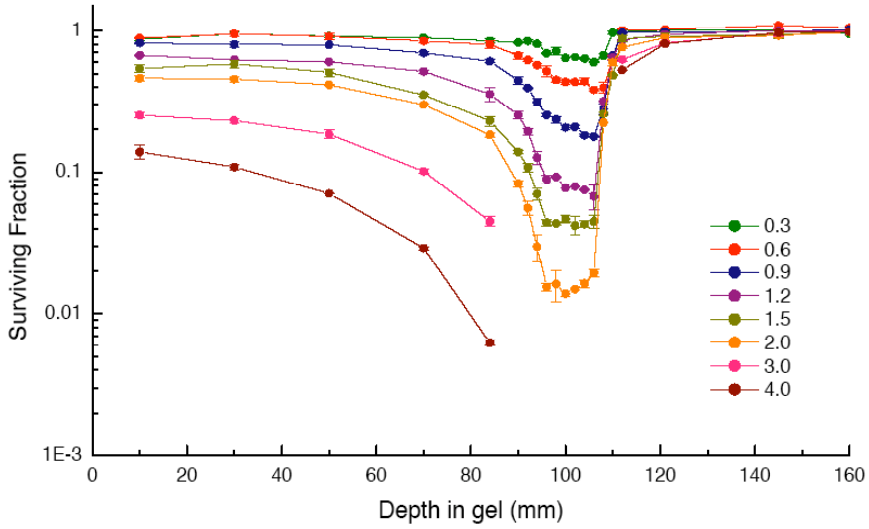

Figure 3: Survival fraction vs. depth in the target for V79 Chinese Hamster cells irradiated with carbon ions

The cell kill in the plateau region is noticeable higher for carbon ions than for antiprotons at similar plateau dose. This is due to the elevated RBE of carbon ions already in the entrance channel. Also noticeable is the earlier and more gradual increase of cell kill for carbon ions compared to antiprotons.

Figure 4 shows the results of our analysis for the carbon ion experiment. Defining the plateau as data points 1 and 2 and the peak as points 9 – 14 of the depth survival curve we can plot survival vs. absolute dose for peak and plateau. In addition we plot survival vs. dose for a reference X-ray source with low LET and RBE of 1. Using a survival rate of 10% we extract the $RBE_{0.1}$ for carbon ions as 1.38 in the plateau and 2.17 in the peak.

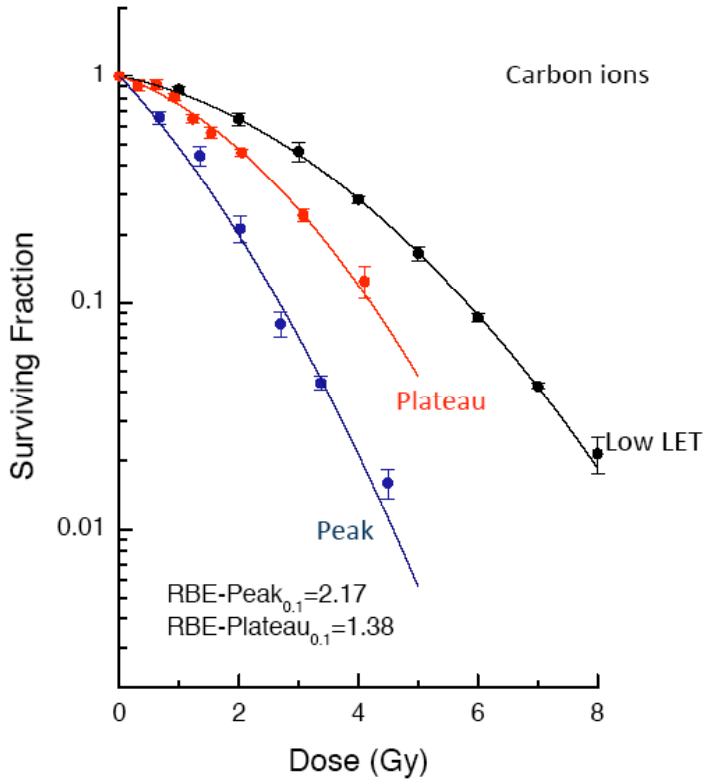

Figure 4: Survival fraction vs. absolute for V79 Chinese Hamster cells irradiated with carbon ions. By comparing the dose needed to achieve a survival of 10% using low LET X-rays to the dose needed when using carbon ions we extract a relative biological efficiency of 1.38 in the plateau and 2.17 in the peak.

Figure 5 shows the same analysis for the antiproton runs. Here the plateau is defined as points 1 – 4 (due to the poorer statistics and the weaker incline with depth we chose more points than in the carbon case) and the peak as points 1 – 13. Varying these choices by a few points did not significantly affect the outcome. Within the limits of the statistical quality of the data points and the uncertainty of absolute dose estimation (using FLUKA together with the number of antiprotons delivered from the AD to the DEM line and the beam profile as measured with the radiochromic film) we reach the preliminary

conclusion that the RBE in the plateau region of antiprotons is consistent with the value of 1 as normally used for protons in radiotherapy planning and that the RBE averaged over the SOBP is 1.54. If more data points are obtained in the plateau region we could cross check the dose estimation assuming that the antiproton RBE for plateau is equal for protons and antiprotons. Also, a few more points in the peak at intermediate dose would lend more significance to the fit of the survival curve to the data.

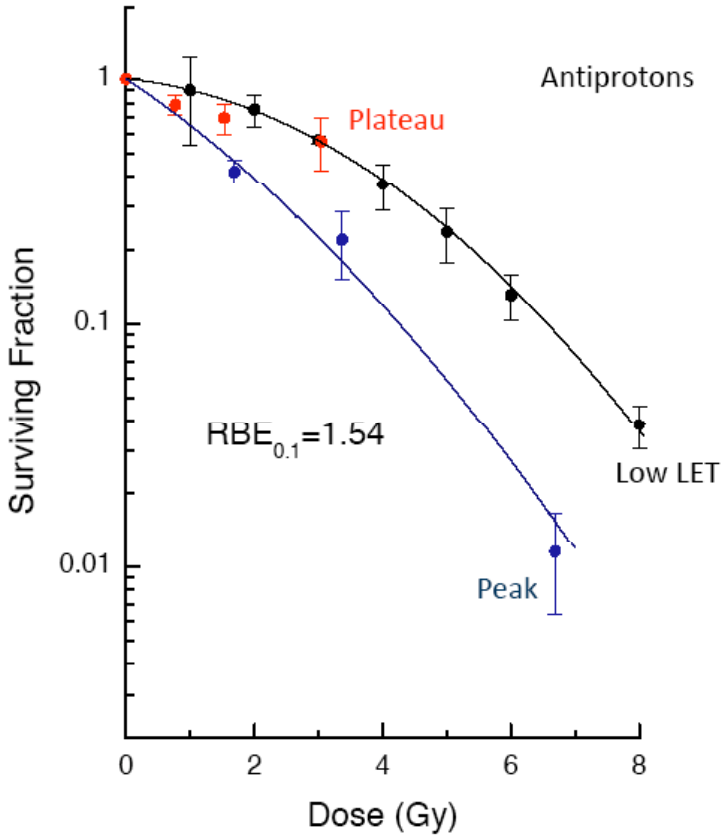

Fig. 5: Survival vs. dose for Chinese Hamster cells irradiated with an antiproton beam of 502 MeV/c energy at the DEM line.

The preliminary analysis shown here continues to support the radiobiological interest in antiproton beams, but a more complete data set is necessary to validate these findings and produce better quantitative results.

II. **Dosimetry Studies:**

To interpret a measured response of a biological system exposed to a beam of hadrons in terms of dose deposition, knowledge of the Relative Biological Effectiveness (RBE) for the particular beam of particles is necessary. Similarly, for a radiation detector the

relative effectiveness (RE) is relating the observed detector response with dose deposition.

Attempts to measure the RBE directly in the peak region of an antiproton beam so far have been problematic, since dosimetry of the antiproton depth dose curve is difficult due to the unknown dosimeter response. Ionization chambers behave non-linear due to volume recombination arising from the pulsed nature of the antiproton beam available at CERN. Measurements using Boag's theorem correcting for recombination effects have been performed during the October 2007 run and a publication on this is in preparation. (see appendix C for a preliminary draft of this paper).

We also performed a set of measurements with Alanine detectors and compared the results with simulations using the particle energy spectrum calculated by FLUKA, and using the track structure model of Hansen et Olsen for conversion of calculated dose into response. Good agreement was observed between the measured and calculated relative effectiveness although a slight underestimation of the calculated values in the Bragg peak remains unexplained. The model prediction of response of alanine towards heavy charged particles encourages future use of the alanine detectors for dosimetry of mixed radiation fields. (see appendix D for a draft of this paper to be submitted).

III. **Beam Time Request:**

To augment the existing data and to allow a full analysis of our data as needed for a publication of this work in a radiobiological journal we plan to perform a second set of irradiations with the same beam energy. Besides filling in missing data points it will also constitute a repeat measurement, which is considered a standard requirement in biological measurements as results can depend on many environmental parameters.

We plan to do a full dosimetric study of the beam prior to the irradiation of any biological samples using data from our ionization chambers, radiochromic film samples, beam current monitors in the AD and at the exit of the DEM line. This will require approximately 48 hours of beamtime, allowing some time for the initial beam development work to be performed by the CERN team. Past experience has shown that this is a critical step in the experimental cycle and cannot be underestimated.

The actual irradiation work then must be completed within a 36 hour time frame for a single set of measurements. If time permits (assuming a smooth operation of the accelerator) we would also like to perform a set of irradiations of human cells, as performed last October, to finish these measurements through a biological control measurement. At this time we are analyzing the data from last October as we needed to wait for the results of the cell survival measurements to decide on the exact analysis protocol. These data will be available prior to October and will allow us to define and decide on the details of this irradiation. Due to the same constraints on sample lifetime, this will also be restricted to 36 hours maximum.

The overall program can be completed in one week of running. In order to impact the other experiments as minimal as possible we request to be granted the last week of running time at the AD as last year. With the biological preparations necessary and considering the limited survival time of the samples once the cells have been harvested and embedded in gelatin, a precise schedule must be established early on. The actual irradiation time can then be adjusted by a few days within the week by waiting until the beam development is completed and dosimetry has been fully established before preparing the actual samples from cell cultures started a few weeks beforehand.

Any limited down time between experiments can be used beneficially to continue our studies on dosimetry issues.

Appendix A: Current list of Collaborators in AD-4

Aarhus University, Dept. of Phys. & Astronomy, DK-Aarhus C, Denmark
Helge KNUDSEN, Soren PAPE-MØLLER, Ulrik UGGERHØJ

Aarhus University Hospital , Nørrebrogade 44, DK-8000 Aarhus, Denmark
Jan ALSNER, Niels BASSLER, Jens OVERGAARD, Jorgen PETERSEN

CERN, Division EP, CH-1211Geneva, Switzerland
Michael DOSER

David Geffen School of Medicine at UCLA, Los Angeles, CA 90095, USA
John J. DeMARCO, Keisuke S. IWAMOTO, William H. McBRIDE

Deutsches Krebsforschungszentrum (DKFZ), 69120 Heidelberg, Germany
Niels BASSLER, Oliver JÄKEL

Geneva University Hospital, 1 rue Michel Servet, CH-1211 Geneva, Switzerland
Gerd BEYER, Oliver HARTLEY, Osman RATIB

University of Maastricht, Res. Inst. Growth and Development, The Netherlands
Bradly G. WOUTERS

University of Montenegro, Nikca od Rovina 53, Podgorica, Montenegro
Dragan HAJDUKOVIC, Sandra KOVACEVIC, Danijela SCEPANOVIC

University of Nebraska Medical Center, Omaha, NE 68198, USA
Timothy SOLBERG

University of New Mexico, Dept. of Phys. & Astr., Albuquerque, NM 87131, USA
Michael H. HOLZSCHEITER

Vinca Institute of Nuclear Sciences, 1101 Belgrade, Serbia & Montenegro
Sanja VRANJES

Appendix B:

Radiotherapy and Oncology 81 (2006) 233–242
www.thegreenjournal.com

Antiprotons

The biological effectiveness of antiproton irradiation

Michael H. Holzscheiter[a], Niels Bassler[b,h,i], Nzhde Agazaryan[c], Gerd Beyer[d], Ewart Blackmore[e], John J. DeMarco[c], Michael Doser[f], Ralph E. Durand[g], Oliver Hartley[d], Keisuke S. Iwamoto[c], Helge V. Knudsen[b], Rolf Landua[f], Carl Maggiore[a], William H. McBride[c], Søren Pape Møller[b], Jørgen Petersen[h,i], Lloyd D. Skarsgard[g], James B. Smathers[c], Timothy D. Solberg[c], Ulrik I. Uggerhøj[b], Sanja Vranjes[j], H. Rodney Withers[c], Michelle Wong[g], Bradly G. Wouters[k,*]

[a]*Pbar Labs, LLC, Santa Fe, NM, USA,* [b]*Deparment of Physics & Astronomy and ISA, University of Aarhus, Aarhus, Denmark,* [c]*David Geffen School of Medicine at UCLA, Los Angeles, CA, USA,* [d]*Centre Medicale Universitaire, Geneva, Switzerland,* [e]*TRIUMF, Vancouver, BC, Canada,* [f]*CERN, PH Department, Geneva, Switzerland,* [g]*British Columbia Cancer Research Centre, Vancouver, BC, Canada,* [h]*Department of Medical Physics, and* [i]*Department of Experimental Clinical Oncology, Aarhus University Hospital, Aarhus, Denmark,* [j]*Vinca Institute of Nuclear Sciences, Belgrade, Serbia and Montenegro,* [k]*Department of Radiation Oncology (Maastro Lab), GROW Research Institute, University of Maastricht, The Netherlands*

Abstract

***Background and purpose*: Antiprotons travel through tissue in a manner similar to that for protons until they reach the end of their range where they annihilate and deposit additional energy. This makes them potentially interesting for radiotherapy. The aim of this study was to conduct the first ever measurements of the biological effectiveness of antiprotons.**

***Materials and methods*: V79 cells were suspended in a semi-solid matrix and irradiated with 46.7 MeV antiprotons, 48 MeV protons, or ^{60}Co γ-rays. Clonogenic survival was determined as a function of depth along the particle beams. Dose and particle fluence response relationships were constructed from data in the plateau and Bragg peak regions of the beams and used to assess the biological effectiveness.**

***Results*: Due to uncertainties in antiproton dosimetry we defined a new term, called the biologically effective dose ratio (BEDR), which compares the response in a minimally spread out Bragg peak (SOBP) to that in the plateau as a function of particle fluence. This value was $\sim$3.75 times larger for antiprotons than for protons. This increase arises due to the increased dose deposited in the Bragg peak by annihilation and because this dose has a higher relative biological effectiveness (RBE).**

***Conclusion*: We have produced the first measurements of the biological consequences of antiproton irradiation. These data substantiate theoretical predictions of the biological effects of antiproton annihilation within the Bragg peak, and suggest antiprotons warrant further investigation.**

Keywords: Antiproton; RBE; Particle irradiation; High LET

For conventional photon irradiation, the maximum dose that can be delivered to a tumor is limited by the tolerance of irradiated adjacent normal tissues. Several technological improvements in radiation delivery, including intensity-modulated radiotherapy (IMRT), have made it possible to confine the high-dose region to almost any target volume of interest and thus reduce the dose to adjacent tissues [1–3]. However, even with these techniques, normal tissue tolerances can prevent delivery of a dose sufficient to achieve tumor cure. IMRT also results in a larger total body exposure and thus an increased risk of secondary cancers [4]. For many types of tumors, this has led to unacceptably low tumor control probability (TCP) and to high levels of morbidity. An alternative approach involves the use of protons and other heavier ions [5–8]. For these charged particles, both the amount and rate of energy deposition increase dramatically as the particle nears the end of its range. This results in a large enhancement in absorbed dose at a precise depth in tissue (the Bragg peak) compared with the dose deposited at the entrance to the body (the

0167-8140/$ - see front matter doi:10.1016/j.radonc.2006.09.012

plateau). For treatment purposes, the position of the Bragg peak needs to be spread out to cover the tumor volume and the production of such a spread-out Bragg peak (SOBP) results in a build up of plateau dose and hence a reduction in the ratio of dose in the SOBP relative to the plateau. However, in contrast to photons, the dose in the SOBP that covers the tumor volume remains larger than that in the normal tissue entrance region. High linear energy transfer (LET) particles such as carbon ions also produce a much higher ionization density in the Bragg peak region and consequently an increase in the relative biological effectiveness (RBE) of the dose deposited in the tumor [9–11]. This provides a potential further therapeutic advantage, especially for tumors that have a large hypoxic fraction or for those that are resistant to conventional radiation [12]. Furthermore, since very little dose is deposited distal to the Bragg peak, charged particles are ideally suited for treatments of tumors close to radiosensitive regions. These favorable physical and biological characteristics have led to recent developments of proton and heavy ion cancer therapy centers worldwide.

Conversion of the mass of a proton–antiproton pair during annihilation constitutes the highest density energy source currently available. This has led to a number of proposals for practical applications of antiprotons, including radiotherapy, which is feasible with current antiproton production technology [13]. Like other charged particles, antiprotons deposit most of their kinetic energy near the end of their path in the Bragg peak. In addition, as an antiproton comes to rest it annihilates, depositing additional energy in the form of particles that may have a significantly enhanced biological effectiveness [14]. The majority of the total annihilation energy of 1.88 GeV is carried away by high-energy pions, neutrons and γ-rays. We have estimated (unpublished data) that the dose deposition from these particles is of a similar magnitude to that reported for a passively degraded proton beam [4]. However, at the Bragg peak it has been estimated that antiprotons deposit an additional 30 MeV within a few millimeters of the annihilation vertex [15]. The only experimental data relevant to the application of antiprotons for biological purposes were produced by Sullivan [16], who measured the relative physical dose deposition in the plateau and the Bragg peak regions for antiprotons at the low energy antiproton ring (LEAR) at CERN. He found that although the additional local dose deposited is small compared to the total annihilation energy, it does represent an approximate doubling of the physical dose deposited per particle in the Bragg peak compared to protons. Furthermore, the RBE of this additional dose is likely to be significantly higher than that for protons because it is due partly to recoiling heavy fragments produced in the annihilation event with short range and high LET. The remainder of the annihilation energy that is carried away,outside of the body, could potentially be used for real-time imaging of the dose distribution.

To date there has been no attempt to assess the biological effects of antiprotons. This stimulated us to initiate an experiment, AD-4/ACE [17,18], running at the antiproton decelerator (AD) at CERN, to measure the biological effects of antiproton irradiation and compare it to the results achievable with protons.

Materials and methods

Beam characteristics

The AD at CERN delivered a 200–500 ns beam pulse containing approximately 3×10^7 antiprotons every 85 s. For our experiment the extraction energy was 46.7 MeV. In order to spread the Bragg peak we used a ridge filter consisting of a plastic sheet machined with a matrix of pixels $\sim$1 mm^2 in area. Three pixel thicknesses (1, 1.8 and 2.6 mm) were used at a ratio of 41:31:28 to create a SOBP as smooth as possible over a distance of slightly more than 2.5 mm. The degrader was placed 25 cm upstream of the target so that the lateral straggling together with the free drift in air would remove any radial dose inhomogeneity from the degrader in the samples. A schematic of the set-up is shown in Fig. 1.

For proton irradiation, we utilized the treatment facility located at TRIUMF, details of which have been previously published [19]. The energy was reduced to 48 MeV with a range shifter to closely match the energy of the antiproton beam. The proton Bragg peak was also spread out over an area slightly larger than 2.5 mm using a two-step rotating wedge filter in order to create a dose profile which matched that of the antiproton as close as possible.

For ^{60}Co irradiation, a Theratron unit at the Vancouver Cancer Centre was used as described previously [19].

Dosimetry

Due to the pulsed nature of the antiproton beam it was not possible to use currently available dosimetry equipment to measure absorbed dose. The large number of antiprotons delivered in such a short period of time leads to saturation, non-linearity and unreliability of conventional equipment such as ionization chambers. Thus, in order to estimate the absorbed dose and the relative depth dose profile we carried out a Monte Carlo simulation based on measurements of antiproton fluence using the MCNPX code [20]. Antiproton fluence was monitored using two independent methods. After the ridge filter the antiproton beam passed through a current monitor (Bergoz[1] BCM/ICT) capable of integrating a pulse with rise times as short as a few picoseconds without significant loss. The voltage was then held level for about 400 μs for read-out. The signal processor used two integrating windows to correct for baseline noise and therefore achieved high accuracy for low beam current. In our set-up the sensitivity was 1 mV/6.3×10^5 antiprotons, resulting in a typical read-out of 50 mV per pulse. The noise was less than 5 mV, allowing a fluence measurement to within 10%. We also received a signature from the accelerator on the number of antiprotons having left the ring upon ejection, which was typically within 20% of the ICT measurement indicating a high-transfer efficiency to our experiment.

In order to estimate the dose with Monte Carlo methods, it was also necessary to determine the radial-beam profile, and thus the fraction of antiprotons that enter the biological sample. We monitored the integrated beam profile using GAF chromic film, which darkens in a linear way with dose. Because the sensitivity is low, it was necessary to integrate

[1] BERGOZ Instrumentation, Espace Allondon Ouest, 06130 Saint Genis Pouilly, France.

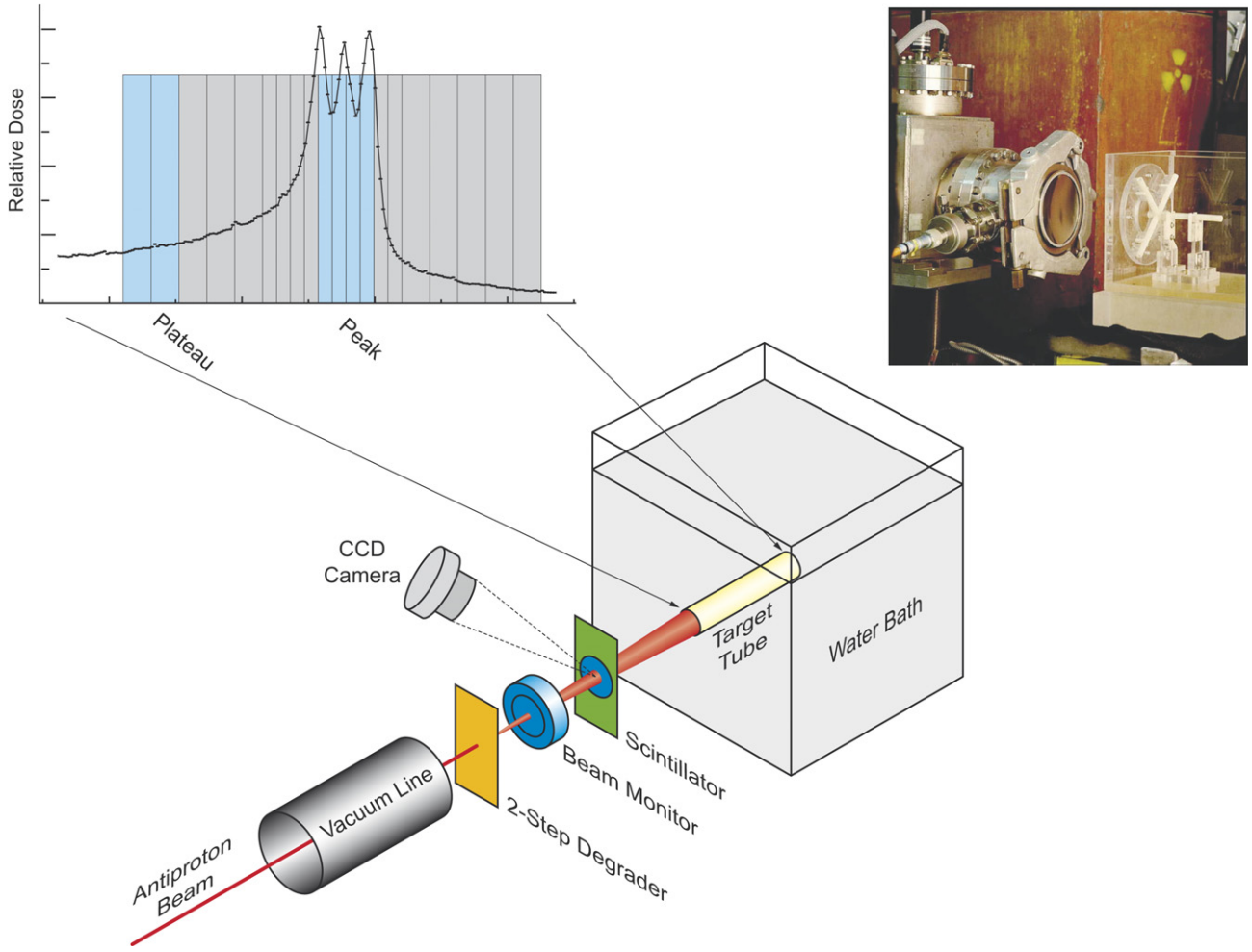

Fig. 1. Schematic set-up of the antiproton experiment. The antiproton beam leaves the accelerator vacuum through a thin titanium window, passes through a two-step ridge filter, a beam current monitor and a scintillator before entering a plexiglass tank containing a glycol/water mixture and the biological sample (see photo inset upper right). Also shown are the antiproton dose profile and the slicing protocol for extracting cell survival data after the irradiation.

over 1–2 h. To monitor individual pulses, we developed a system consisting of a thin sheet of BC-400 scintillator material intercepting the beam without affecting energy or straggling significantly. This material was placed near the entrance to the phantom and viewed by a sensitive CCD camera.[2] To reduce noise, the camera was synchronized with the arrival of the pulse, and the signal was sufficient to obtain the beam profile and to determine the centroid and diameter of a single shot from the AD. This system also allowed us to adjust the beam position in sub-millimeter increments. Only the central part of the Gaussian-shaped beam was used to ensure a radial variation of less than 5%.

For protons, the delivered dose was measured by a calibrated transmission chamber and relative depth–dose measurements were carried out with a parallel plate ionization chamber.

[2] APOGEE Instruments Inc., KX1E Digital Imaging System, comprising a TE cooled camera head with Grade 2 Kodak KAF-0401E CCD.

Measurement of clonogenic survival

We chose to use V79-WNRE cells in these studies because this cell line has been used previously to quantify the biological characteristics of other particle beams [19]. We employed a modified form of the sliced-gel technique of Skarsgard and co-workers [19,21] coupled with the cell sorter survival assay, details of which are published elsewhere [19,22]. Briefly, cells were cultured in MEM supplemented with 10% fetal bovine serum and maintained in exponential growth. Cells were harvested with trypsin, and re-suspended at 2×10^6 cells/ml in MEM containing 20% FBS and 12% gelatin (gel/medium). At 37 °C, this was a viscous fluid and for proton and antiproton irradiations, was poured into ABS (acrylonitrile butadiene styrene) plastic tubes of 0.6 cm inside diameter and 18 cm length, with a piston located so as to accommodate a 6-cm deep cylinder of gel/medium. For ^{60}Co irradiation, 0.5–1 ml samples of the cell/gel suspension were deposited into 5 ml plastic test tubes. After solidification at 4 °C the tubes were sealed and stored on ice.

For irradiation, sample tubes were placed with their axis collinear with the beam axis, in a circulating, refrigerated bath containing a 19.3% glycerol/water solution. The

densities of materials encountered by the beam (ABS tube, gel/medium, glycerol/water) were carefully chosen to produce identical stopping powers throughout the entire phantom. The cells were maintained at 2 °C throughout the irradiation procedure and were kept on ice prior and subsequent to irradiation. This maintained the spatial organization of the cells, and also avoided dose-rate effects that would have otherwise confounded measurements (individual sample antiproton exposures were as long as 16 h). Only the central part of the antiproton beam was used to irradiate the cell sample tube, thus assuring an intensity variation across the sample of less than 5%. After irradiation, the gel was extruded from the tube and cut into slices of 0.5 or 1 mm thickness. These slices were melted in warm culture medium and a cell sorter was then used to sort an accurately known number of cells from each sample. Two to three sorts from each slice were plated into individual 100-mm Petri dishes with 14 ml of culture media and allowed to form colonies (defined as >50 cells) for 6–7 days. A sufficient number of cells was plated to produce ~400–500 colonies per dish. Three slices upstream of the SOBP which received zero primary dose were used to measure the plating efficiency (PE).

For comparison purposes we also measured the clonogenic survival response of V79 cells in the gelatin-matrix to ^{60}Co irradiation. This served as both a reference to measure the RBE for protons and also allowed us to control for any minor variations in the radiosensitivity of the cells between experiments. For antiproton experiments, samples were prepared at CERN and irradiated in Vancouver after transport. For proton experiments, ^{60}Co samples were irradiated at times similar to the proton samples.

Determination of RBE and BEDR

The goal of our experiments was to obtain an estimate of the biological effect of antiprotons. Conventionally, this property would be the RBE, which is equal to the ratio of absorbed dose between the conventional and test irradiation producing the same level of survival. For proton irradiation it was possible to determine RBE because we have a reliable measure of dose. RBE was calculated as the ratio of ^{60}Co to proton doses which resulted in the same level of cell survival. Dose values were determined from linear quadratic (LQ) fits to the survival data.

It was not possible to calculate a similar RBE for antiprotons because we did not have a reliable measure of the absorbed dose. Thus, it was necessary to design comparative experiments in such a way that measurement of absolute dose was not required. To do this we compared survival responses obtained in the SOBP with those obtained in the plateau following delivery of a known number of particles (fluence). Because the dose in the plateau and the SOBP are directly proportional to the fluence, it is possible to compare the responses without knowing the conversion factor from fluence to dose. We defined a new term called the biologically effective dose ratio (BEDR), equal to the ratio of plateau to SOBP fluences required to produce a defined level of survival.

$$\mathrm{BEDR} = \frac{\mathrm{Fluence}_{\mathrm{plateau}}}{\mathrm{Fluence}_{\mathrm{peak}}},$$

where $\mathrm{Fluence}_{\mathrm{plateau}}$ and $\mathrm{Fluence}_{\mathrm{peak}}$ are the different fluences that produce the same level of cell survival. It can be shown that BEDR is numerically equal to

$$\mathrm{BEDR} = F\frac{\mathrm{RBE}_{\mathrm{peak}}}{\mathrm{RBE}_{\mathrm{plateau}}},$$

where F is the ratio of the physical dose deposited in the SOBP to that deposited in the plateau.

Results

Physical dose

The axial physical dose profiles of the proton and antiproton beams are shown in Fig. 2. For protons, this figure represents the measured relative dose as a function of depth in water and for antiprotons it is a Monte Carlo estimate based on conversion from particle fluence measurements. The modulation of dose in the Bragg peak results from the use of the discrete two-step degrader with a step size comparable to the width of the pristine Bragg peak for this energy. As expected, the peak to plateau dose ratio is much larger for antiprotons than for protons. Defining a point 7 mm upstream as the plateau yields a measured dose ratio of 2.0 for protons and an estimated 4.0 for antiprotons. The positions and widths of gel slices used to measure clonogenic survival in different regions of the beam are also shown.

Because samples were irradiated over a 24-h period at CERN and then transported to Vancouver, the cells were maintained in gel at cold temperatures for 42–54 h. The PE measured from each sample tube, as well as the PE from several unirradiated controls allowed us to monitor the consequences of this exposure (see Fig. 3a). Although, there was a small trend towards increased toxicity with time (a drop in PE from ~0.7–0.6), the PE remained high throughout the experiment and comparable to that measured previously[19]. Fig. 3b shows the ^{60}Co survival curves determined during both the proton experiment at TRIUMF and the antiproton experiment in CERN. The similarity of these two responses also indicates that the long exposure to gel did not significantly affect radiosensitivity.

Survival data

Fig. 4a and b show the clonogenic survival determined from individual gel slices plotted as a function of depth throughout the proton and antiproton beams. The depth in gel has been converted to its stopping-power equivalent depth in water. All material in front of the gel (the gel cap, tank window, and other materials) has also been converted to water equivalent depth and included so that the plots represent the total particle range.

For the proton experiment, cell survival was determined from 20 individual slices as a function of depth in each of eight sample tubes receiving a different dose to the SOBP. The dose range to the SOBP was 1–14Gy and resulted in survival measurements over 1 log in both the peak and plateau regions. The survival responses are in good agreement with expectations from the measured dose distributions shown in the upper panel. The steep dose gradient beyond the edge

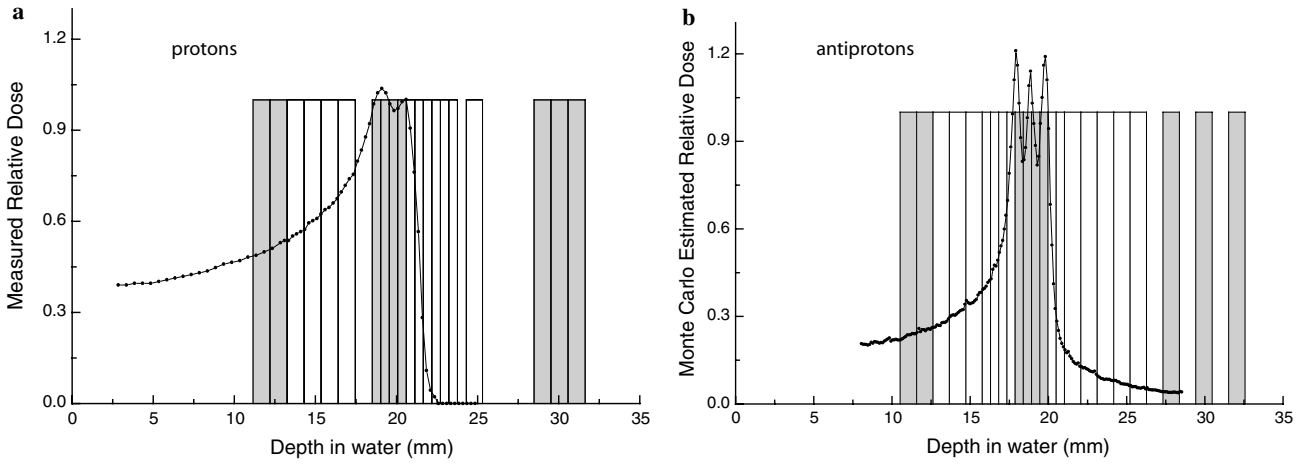

Fig. 2. Physical dose profiles and slicing protocol. The measured physical dose along the axis of the range-modulated proton beam at TRIUMF (a) and the Monte Carlo estimated physical dose along the axis of the range-modulated antiproton beam at CERN (b) are shown as a function of depth in water. The SOBP is approximately 2.5 mm in width. Also plotted are the positions and widths of gel slices from which clonogenic survival was determined. Four positions in the peak (2 mm total width), and two positions 7 mm upstream from the peak center (2 mm total width) were used to determine average values for the SOBP and plateau, respectively (shaded areas). Three slices beyond the Bragg peak were used to determine plating efficiency.

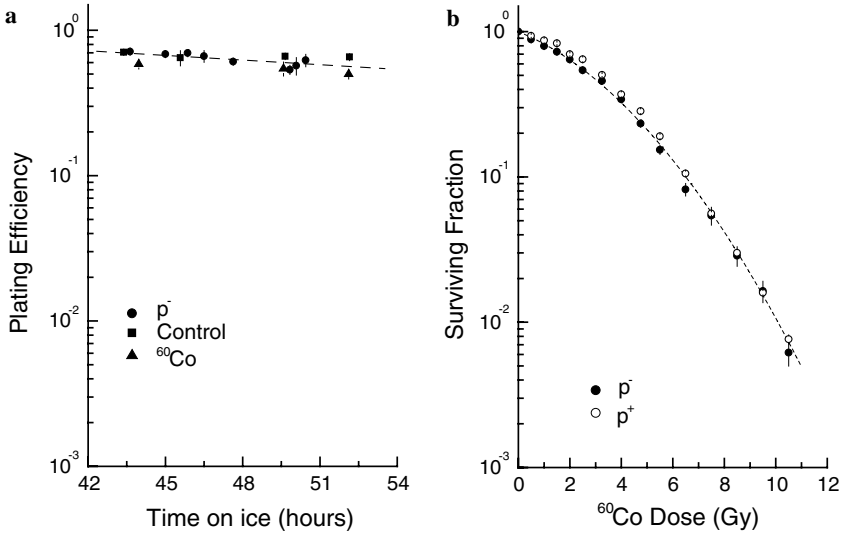

Fig. 3. Plating efficiency and radiosensitivity during extended exposure to gelatin. The plating efficiency of V79-WNRE cells as a function of time at 0 °C in the gelatin matrix from samples used during one of the antiproton experiments (a). Plating efficiency was determined from individual sample tubes that received antiproton irradiation (p^-), or from untreated control tubes (control). Plating efficiencies of the ^{60}Co control samples are also shown (^{60}Co). The clonogenic survival of V79-WNRE cells is shown as a function of ^{60}Co dose (b). These ^{60}Co-response curves were derived from samples prepared during the antiproton experiment at CERN (p^-) and during the proton experiment at TRIUMF (p^+).

of the SOBP allowed us to verify the positioning of the sample tube to less than 0.5 mm.

Fig. 4b shows similar data obtained following irradiation with antiprotons. Because it was not possible to measure absolute dose, we used the estimates based on measured antiproton fluence and Monte Carlo models. Survival data were determined at 23 positions in depth for six individual sample tubes irradiated with estimated peak doses between 1 and 25Gy. These data demonstrate a much higher difference between the peak and plateau regions. Interestingly, the non-uniform dose in the SOBP predicted by Monte Carlo analysis is reflected in these measurements.

RBE and BEDR

In Fig. 5a, we have plotted the survival as a function of absorbed dose for both proton and ^{60}Co irradiation. The proton dose responses were constructed from the data shown in Fig. 4a. The survival in the peak region was calculated from the average of the four 0.5 mm slices located within the SOBP and the survival in the plateau was calculated as the

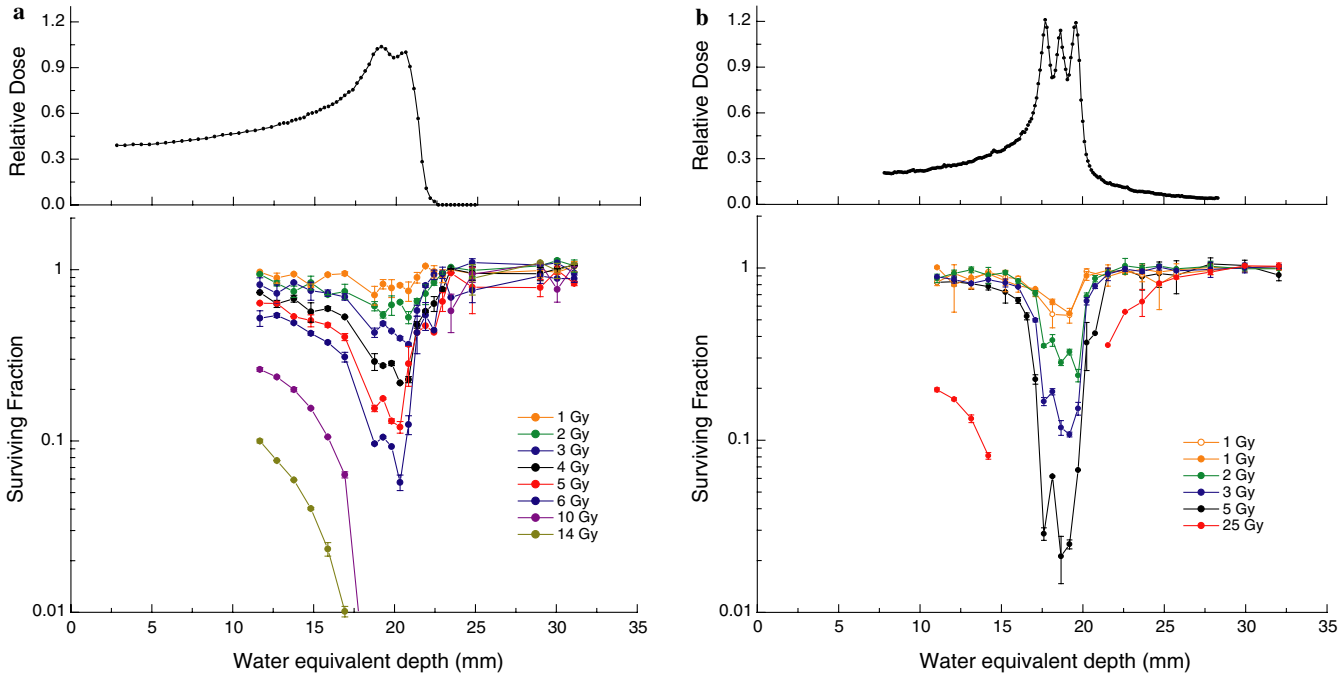

Fig. 4. Clonogenic survival response to antiprotons and protons. The clonogenic survival of V79-WNRE cells is plotted as a function of water equivalent depth along the axis of the proton beam (a) and antiproton beam (b). Survival was measured in 20 individual gel slices after proton irradiation and in 23 slices after antiproton irradiation in individual tubes irradiated with a range of peak doses. Each line represents a single tube irradiated with the measured proton (a) or estimated antiproton (b) dose to the SOBP. For reference, the physical dose profiles are shown in the upper frames.

average of two 1 mm slices located 7 mm upstream (see also Fig. 2a). The relative dose in the plateau at this point was 51% of that in the peak. The resulting dose response in the plateau is indistinguishable from that for ^{60}Co irradiation, and thus the RBE in this region is 1. The radiation sensitivity of cells irradiated in the SOBP is significantly higher. We used the LQ model to fit the ^{60}Co and proton SOBP responses and then calculated the RBE at different levels of survival (Fig. 5a). The RBE_{20} (RBE at a surviving fraction of 20%) for the proton SOBP is equal to 1.2, in good agreement with previous measurements with this system [19].

In Fig. 5b and c, we have replotted the plateau and SOBP survival as a function of particle fluence rather than absorbed dose. In this manner, the response in the SOBP appears far more sensitive than in the plateau (compare proton data in Fig. 5a and b). This arises because the absorbed dose per particle in the SOBP is higher (for protons ~2-fold) and additionally because the RBE in the SOPB is higher. These fluence based survival responses were then fit using the LQ equation, and the resulting parameters used to calculate the BEDR. This value is equal to the ratio of fluences in the plateau and the peak that give the same level of cell survival. At 20% survival the BEDR for protons is 2.4.

The survival responses in the SOBP and plateau regions of the antiproton beam are shown as a function of fluence in Fig. 5c. These plateau data were calculated as the average survival from two 1 mm slices located 7 mm upstream of the SOBP, and the SOBP response is taken from the average of the four 0.5 mm slices located within the SOBP region. Data extracted from the data set shown in Fig. 4b are labeled as Exp1. Also shown in Fig. 5c, are data obtained from a smaller experiment carried out 3 months prior (Exp 2). The BEDR for antiprotons determined from LQ fits to these data is shown in the lower frame of Fig. 5c. At 20% survival the antiproton BEDR is equal to 9.0, or about 3.75 times higher than for protons.

Antiproton RBE

Although, we could not directly measure antiproton RBE, it is possible to make an estimate of this value based on the measurements presented so far. The ratio of BEDR for antiprotons to protons is equal to:

$$\frac{BEDR(p^-)}{\mathrm{BEDR}(p^+)} = \frac{F(p^-)}{F(p^+)} \cdot \frac{\mathrm{RBE}(p^-)_{\mathrm{peak}}/\mathrm{RBE}(p^-)_{\mathrm{plateau}}}{\mathrm{RBE}(p^+)_{\mathrm{peak}}/\mathrm{RBE}(p^+)_{\mathrm{plateau}}}.$$

This can be rearranged to determine the RBE for antiprotons in the SOBP:

$$\mathrm{RBE}(p^-)_{\mathrm{peak}} = \frac{\mathrm{BEDR}(p^-)}{\mathrm{BEDR}(p^+)} \cdot \frac{F(p^+)}{F(p^-)} \cdot \frac{\mathrm{RBE}(p^-)_{\mathrm{plateau}}}{\mathrm{RBE}(p^+)_{\mathrm{plateau}}} \cdot \mathrm{RBE}(p^+)_{\mathrm{peak}}.$$

The only value in this equation that has not been estimated or measured is the antiproton RBE in the plateau. However, this value is equivalent to the proton plateau RBE provided that in-fight annihilation dose is insignificant. We estimated the consequence of in-flight annihilation by finding an accurate universal fit to all measured annihilation cross sections known to us, from which we calculated the effect in our specific case [23]. Using our knowledge of the stopping power of antiprotons we then calculated the number of remaining antiprotons, and the electronic energy deposited along the beam path (Fig. 6a). Here, we have ignored elastic

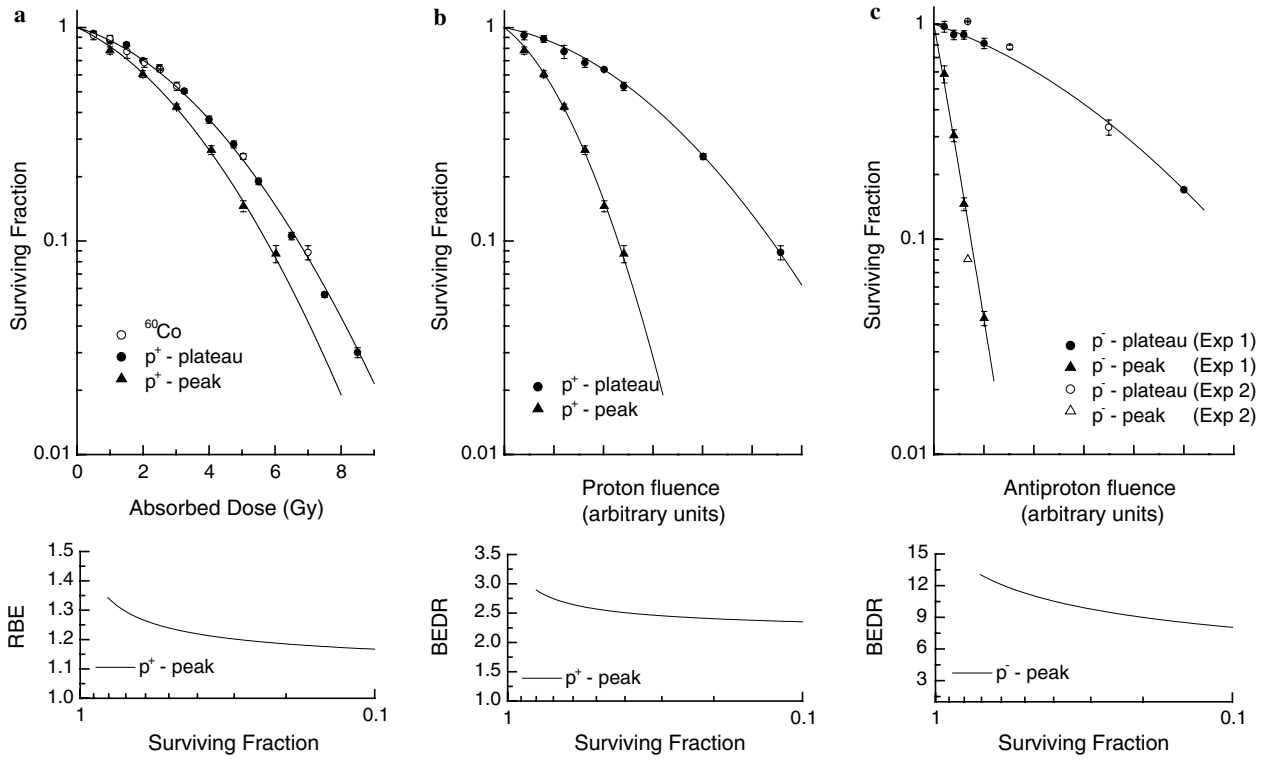

Fig. 5. Determination of RBE and BEDR. The average survival of cells within the SOBP and plateau region of the proton beam are plotted as a function of absorbed dose (a, upper frame). These data were fit with the LQ model, and the resulting parameters used to calculate the RBE as a function of surviving fraction (a, lower frame). In (b), the same proton data from (a) are plotted as a function of proton fluence (upper frame) and fits to these data were used to calculate the BEDR (lower frame). In (c, upper frame), the average survival of cells within the SOBP and plateau region of the antiproton beam are plotted as a function of antiproton fluence. Fits to these data were used to calculate the antiproton BEDR (c, lower frame). In the text, BEDR and RBE values are quoted at a survival of 20%. At this level of survival, the BEDR for antiprotons is approximately 3.75-fold higher than for protons due to the increased annihilation dose in the SOBP and its higher RBE.

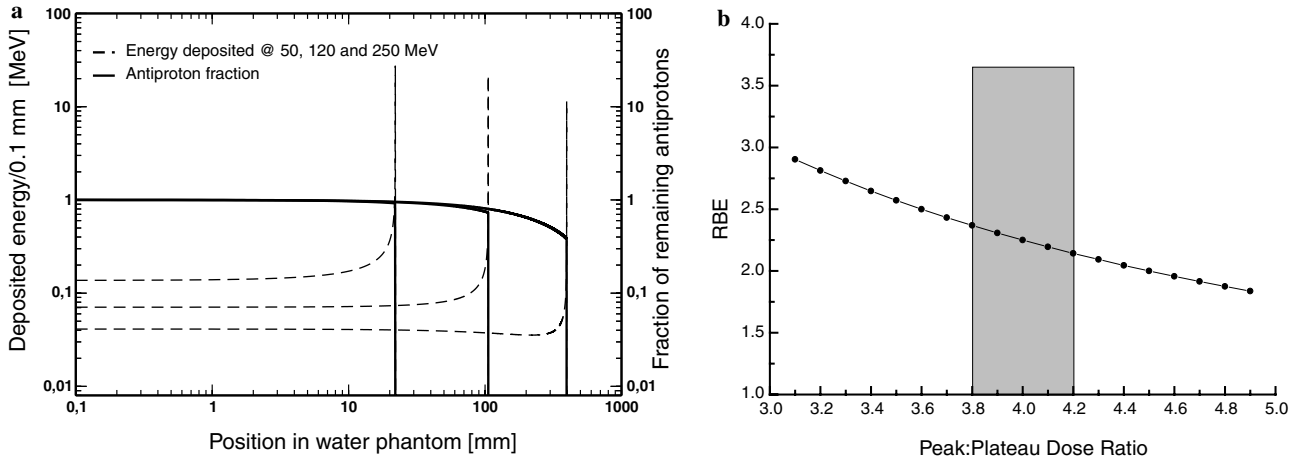

Fig. 6. Estimation of RBE in the antiproton SOBP. The amount of deposited energy along the tracks of 50, 120 and 250 MeV antiprotons passing through water (dashed lines) (a). Also shown in this plot are the remaining fractions of antiprotons for each of these energies (solid curves). In (b) the RBE in the antiproton SOBP has been estimated for different values of the peak to plateau dose ratio. The product of the RBE and this ratio is equal to the measured BEDR. The shaded area represents the best estimate for the dose ratio.

scattering as well as transport of secondary particles and assumed that each annihilation deposits 30 MeV of energy locally. The loss of antiprotons with an initial energy of 50 MeV due to in-flight annihilation is very small (8%) and even for higher energies up to a depth of 40 cm, a distinct Bragg peak remains.

Thus, if we assume equivalent plateau RBE values, the antiproton RBE in the SOBP becomes the following:

$$\mathrm{RBE}(p^-)_{\mathrm{peak}} = \frac{\mathrm{BEDR}(p^-)}{\mathrm{BEDR}(p^+)} \cdot \frac{F(p^+)}{F(p^-)} \cdot \mathrm{RBE}(p^+)_{\mathrm{peak}}.$$

The only value that has not been directly measured in this equation is the dose ratio (F) for antiprotons. However, if we use the Monte Carlo estimate of 4.0 for this value as depicted in Fig. 2b, the antiproton RBE in the SOBP is equal to 2.25. Because we are not completely certain of the Monte Carlo dose estimates we have also plotted in Fig. 6b the relationship between F and the peak RBE for antiprotons that is required to produce the measured BEDR_{20} value of 9.0.

Discussion

The biological effectiveness of antiprotons

The data presented here are the first measurements to date of the biological consequences of antiproton irradiation. The nature of the antiproton beam made it impossible to determine standard dose—response curves that could be compared with low-LET radiation to determine the RBE. We thus defined the BEDR, a new term that is based on comparing the responses in the peak and plateau regions as a function of particle fluence. This value is biologically meaningful, because it represents a direct measurement of the gain in 'biologically equivalent dose' deposited in the Bragg peak region compared to that in the plateau. Since the dose deposition in the plateau is essentially identical for proton and antiproton beams of similar energy, a comparison of the BEDR of protons with that of antiprotons provides a direct measure of the additional biological consequences of annihilation events at the Bragg peak.

At 20% survival the BEDR_{20} for antiprotons was equal to 9.0 and for protons it was 2.4- or 3.75-fold lower. The BEDR for antiprotons increased because of two factors: (i) the increase in the ratio of dose deposited in the SOBP relative to the plateau due to the annihilation dose and (ii) the increase in the RBE of the extra annihilation dose. For protons, the RBE in the SOBP was 1.2 and the peak to plateau dose ratio was 2.0. The product of these two values gives the BEDR value of 2.4. For antiprotons our best estimate of the peak to plateau dose ratio is 4.0-, or 2-fold higher than that for protons. This results in an estimate of the antiproton SOBP RBE of approximately 2.25 provided that the RBE in the plateau region is similar to that for protons. Our estimation of in-flight annihilation dose indicates that this effect is indeed small, suggesting that this assumption is valid. Given the fact that the annihilation dose in the peak accounts for only an estimated 50% of the total dose in this area, an average RBE of 2.25 in this region implies that the RBE for the dose contributed by annihilation must be very high.

Comparison to carbon ions

It would be interesting to compare our measurements with other high LET particles, such as carbon ions. Blakely et al. [9] measured cell survival in pristine peaks of 400 MeV/u carbon ions using the Berkeley Bevalac. Range straggling in this high-energy beam yielded a Bragg peak of stopping width similar to our modulated proton and antiproton beams (~3 mm at 80% of maximum). We estimated the BEDR for this carbon ion beam to be 7.9, using a definition for the plateau point reflecting the situation encountered at CERN (7 mm upstream). However, the much greater range of the carbon ions adds uncertainty to this estimate. Because the gradient on the proximal side of the Bragg peak changes drastically with penetration depth, it is difficult to make a proper choice for the plateau definition. Weyrather et al. [10,11] have also reported RBE values for a range of carbon ion energies. Using SRIM [24] we calculated a dose profile for a pristine carbon beam with a range equivalent to our set-up at CERN and estimated the maximum BEDR from the Weyrather data to be 8.5 (after correcting for the loss of primary ions due to fragmentation). This result is for an unmodulated pristine Bragg peak. Spreading the Bragg peak to a width similar to that in our experiment significantly lowers the peak to plateau-dose ratio and hence the BEDR. We estimated this would reduce the BEDR to ~5. High uncertainties in this analysis have prompted us to begin a comparison measurement for carbon ions using a set-up equivalent to that at CERN.

Another important consideration in the comparison of antiproton irradiation with other high-LET particles is the value of the RBE upstream of the Bragg peak. As discussed above, the RBE for antiprotons in the plateau region is not expected to be different from that for protons. Because the contribution of in-flight annihilation is small, the biological dose deposited outside of the Bragg peak per particle is essentially the same as that for a proton. This would have a significant clinical advantage over other high LET particles such as carbon ions, which have RBE values significantly greater than 1 in the plateau region of the depth-dose curve. As a consequence, it is not possible to use the clinical experience with low-LET radiations to estimate normal tissue tolerances without making an assumption for the RBE. Because high-LET particles often have RBE values that are energy, dose and cell type specific, one must use caution in the application of these particles in the clinic. For antiprotons, because the annihilation dose (high-LET component) would be confined to the tumor, it would be possible to treat using established normal tissue dose tolerances.

Peripheral damage

An important aspect for any new irradiation concerns the biological consequences of dose that may be deposited outside of the primary beam. Initial attempts to assess peripheral damage caused by antiproton annihilation suggest it is quite small. Even for the highest dose used in our experiments, which resulted in a surviving fraction of 20% in the plateau, we observed ~55% survival at only 2 mm distal to the Bragg peak (see Fig. 3). Furthermore, we also made preliminary measurements of clonogenic survival in sample tubes placed perpendicular to the beam at the Bragg peak. These data also indicate that the peripheral dose is small (data not shown). Further experimental studies in the peripheral regions using beams with peaks spread according

to clinically relevant criteria will be required to fully quantify these effects.

Conclusion

In conclusion, our experiment has produced the first direct measurements of the biological consequences of antiproton irradiation. It substantiates theoretical predictions and earlier speculations on the consequences of antiproton annihilation within the Bragg peak [15,25]. For the beams compared in our study, the BEDR for antiprotons was 3.75-fold larger than the BEDR for protons, which represents a substantial increase in effective dose within the SOBP. In a treatment situation, a higher energy beam with a larger SOBP would be required to treat tumors of a reasonable size. As a result, the peak to plateau dose ratio for either a proton or antiproton beam would be significantly reduced, and the comparison would yield a value below the value observed here. However, antiprotons would retain a significant biological dose advantage due to the contribution of both the annihilation dose and its high estimated RBE. In this regard, it is important to note that there are a number of treatment situations in which increases in tumor dose as small as 10–20% can produce significant improvements in outcome.

Future research has to show if the advantages of antiprotons in terms of (a) higher physical dose in the Bragg peak, (b) the increased RBE confined to the Bragg peak and (c) the real-time imaging capability will warrant their serious consideration as an alternative modality for tumor irradiation. At that time it will be necessary to analyze both the technical and financial problems posed by the antiproton production process. While the actual treatment center will be similar to a standard proton center, the production of antiprotons requires accelerating protons to 20–30 GeV. With current technology this requires a synchrotron of about 100–200 m in diameter. Production, capture, storage and delivery of antiprotons will require a number of additional accelerator rings. CERN currently produces a modest amount of antiprotons that suffice for limited biological studies. GSI is planning the construction of a high energy addition to their existing facility which will make available antiprotons useful for irradiation at greater depths at intensities sufficient for standard irradiation times and realistic tumor volumes [26]. This facility could theoretically be used to further evaluate and develop antiproton treatment clinically.

Acknowledgements

The Danish Cancer Society supported the project with a grant. Some of us (N.B., H.V.K., S.P.M., U.I.U.) have been supported by the ICE center under the Danish Science Research Council.

* **Corresponding author. Bradly G. Wouters**, Department of Radiation Oncology, Maastricht Radiation Oncology (Maastro) Lab, GROW Research Institute, USN50/23 University of Maastricht, P.O. Box 616, 6200MD Maastricht, The Netherlands. *E-mail address:* brad.wouters@maastro.unimaas.nl

Received 27 June 2006; received in revised form 6 September 2006; accepted 13 September 2006; Available online 27 October 2006

References

[1] Lof J, Lind BK, Brahme A. An adaptive control algorithm for optimization of intensity modulated radiotherapy considering uncertainties in beam profiles, patient set-up and internal organ motion. Phys Med Biol 1998;43:1605–28.
[2] Group ICW. Intensity-modulated radiotherapy: current status and issues of interest. Int J Radiat Oncol Biol Phys 2001;51:880–914.
[3] Williams PC. IMRT: delivery techniques and quality assurance. Br J Radiol 2003;76:766–76.
[4] Hall EJ. Intensity-modulated radiation therapy, protons, and the risk of second cancers. Int J Radiat Oncol Biol Phys 2006;65:1–7.
[5] Levin WP, Kooy H, Loeffler JS, DeLaney TF. Proton beam therapy. Br J Cancer 2005;93:849–54.
[6] Suit H, Goldberg S, Niemierko A, et al. Proton beams to replace photon beams in radical dose treatments. Acta Oncol 2003;42:800–8.
[7] Schulz-Ertner D, Nikoghosyan A, Thilmann C, et al. Carbon ion radiotherapy for chordomas and low-grade chondrosarcomas of the skull base. Results in 67 patients. Strahlenther Onkol 2003;179:598–605.
[8] Mazeron JJ, Noel G, Feuvret L, Calugaru V, Racadot S. Clinical complementarities between proton and carbon therapies. Radiother Oncol 2004;73:S50–2.
[9] Blakely EA, Tobias CA, Yang TC, Smith KC, Lyman JT. Inactivation of human kidney cells by high-energy monoenergetic heavy-ion beams. Radiat Res 1979;80:122–60.
[10] Weyrather WK, Kraft G. RBE of carbon ions: experimental data and the strategy of RBE calculation for treatment planning. Radiother Oncol 2004;73:S161–9.
[11] Weyrather WK, Ritter S, Scholz M, Kraft G. RBE for carbon track-segment irradiation in cell lines of differing repair capacity. Int J Radiat Biol 1999;75:1357–64.
[12] Svensson H, Ringborg U, Naslund I, Brahme A. Development of light ion therapy at the Karolinska Hospital and Institute. Radiother Oncol 2004;73:S206–10.
[13] Slater JM. Considerations in identifying optimal particles for radiation medicine. Technol Cancer Res Treat 2006;5:73–9.
[14] Kraft G, Scholz M, Bechthold U. Tumor therapy and track structure. Radiat Environ Biophys 1999;38:229–37.
[15] Gray L, Kalogeropoulos TE. Possible biomedical applications of antiproton beams: focused radiation transfer. Radiat Res 1984;97:246–52.
[16] Sullivan AH. A measurement of the local energy deposition by antiprotons coming to rest in tissue-like material. Phys Med Biol 1985;30:1297–303.
[17] Maggiore C, Agazaryan N, Bassler N, Blackmore E, Beyer G, DeMarco JJ, et al. Biological effectiveness of antiproton annihilation. Nucl Instrum Meth B 2004;214:181–5.
[18] Holzscheiter MH, Agazaryan N, Bassler N, Beyer G, DeMarco JJ, Doser M, et al. Biological effectiveness of antiproton annihilation. Nucl Instrum Meth B 2004;221:210–4.
[19] Wouters BG, Lam GK, Oelfke U, Gardey K, Durand RE, Skarsgard LD. Measurements of relative biological effectiveness of the 70 MeV proton beam at TRIUMF using Chinese hamster V79 cells and the high-precision cell sorter assay. Radiat Res 1996;146:159–70.
[20] Waters LS, Hendricks JS, Hughes HG, McKinney GW, Snow EC. Medical Applications of the MCNPX Code. American Nuclear Society, 12th Biennial Radiation Protection and Shielding Division Topical Meeting, Santa Fe, NM, 8-89448-667-5, ANS Order No. 700293 April 14–18, 2002.

[21] Skarsgard LD, Palcic B, Douglas BG, Lam GK. Radiobiology of pions at TRIUMF. Int J Radiat Oncol Biol Phys 1982;8:2127—32.
[22] Durand RE. Use of a cell sorter for assays of cell clonogenicity. Cancer Res 1986;46:2775—8.
[23] Bassler N, Holzscheiter M, Knudsen H, Collaboration AD-4/ACE. Cancer therapy with antiprotons. LEAP, American Institute of Physics, CP796, AIP Conference Proceedings 2005. p. 423—30.
[24] Ziegler JF, Biersack JP, Littmar U. The Stopping and Range of Ions in Solids. New York: Pergamon Press; 2003.
[25] Kalogeropoulos TE, Muratore R. Antiprotons for imaging and therapy. Nucl Instrum Meth B 1989;B40—41: 1322—5.
[26] Gross K, Eschke J. Facility for antiproton and ion research (FAIR). Nucl Phys News 2006;16:5—8.

Appendix C:

The Antiproton Depth Dose Curve in Water

Niels Bassler[a], Michael Holzscheiter[b], Sandra Kovacevic[c]
and the AD4/ACE Collaboration*

June 28, 2007

[a] Department of Experimental Clinical Oncology, Aarhus University Hospital, Aarhus, Denmark
[b]University of New Mexico, Albuquerque, NM, USA
[c]University of Montenegro, Podgorica, Montenegro

*Michael H. Holzscheiter1, Niels Bassler2,3, Jan Alsner2, Gerd Beyer4, John J. DeMarco5, Michael Doser6, Dragan Hajdukovic7, Oliver Hartley4, Keisuke S. Iwamoto5, Oliver Jäkel3, Helge V. Knudsen8, Sandra Kovacevic7, Søren Pape Møller8, Jens Overgaard2, Jørgen B. Petersen2, Osman Ratib4, Timothy D. Solberg9, Sanja Vranjes10, Bradly G. Wouters11.

1 University of New Mexico, Albuquerque, NM, USA 2 Dept. of Medical Physics and Experimental Clinical Oncology, Aarhus University Hospital, Aarhus, Denmark 3 Deutsches Krebsforschungszentrum, Heidelberg, Germany 4 Hospital Universitaire de Geneve, Geneva, Switzerland 5 David Geffen School of Medicine, UCLA, Los Angeles, CA, USA 6 CERN, Geneva, Switzerland 7 University of Montenegro, Podgorica, Montenegro 8 Dept. of Physics & Astronomy and ISA, University of Aarhus, Aarhus, Denmark 9 University of Nebraska Medical Center, Omaha, NE, USA 10 VINCA Institute for Nuclear Sciences, Belgrade, Serbia 11 University of Maastricht, Res. Institute Growth and Development, The Netherlands.

Abstract

1 Introduction

The basic idea in antiproton radiotherapy [1] is to utilize the energy from the antiproton-nucleus annihilation reactions. Antiprotons behave similar as protons at high velocities, but when they slow down, they will be captured by a nucleus and annihilate on its surface. Hereby twice the rest mass of the proton m_p is released (1,88 GeV). The probablity for photo-emission similar to that known from the postiron-electron annihilation is rather small. Instead, in average 4-5 π-mesons are created [2]. The photons observed from the antiproton annihilation arise primarily from π^0 decay, which has a lifetime in the order of 10^{-16} seconds. For antiproton-nuclei reactions, there is a $\gtrsim 85\%$ probablility that one or more antiprotons will strike the nucleus [3]. Those entering the nucleus will start an intranuclear cascade, knocking out light nuclei [4]. When antiprotons enter a chemical compound, consisting of several materials, the majority of the annihilations will take place on high-Z materials [5], e.g. for polystyrene only 1% will annihilate on hydrogen and the rest on carbon. Thus, from antiproton annihilation on e.g. tissue, a particle spectrum is expected, featuring pions, neutrons, protons, deuterons, heavier nuclei and photons. A

few kaons may also be created [6, 7]. Most of the 1,88 GeV released is carried away by the long-ranging particles, but still roughly 30 MeV is beind deposited locally near the annihilation vertex [8]. Even though this sounds disappointingly low [2, 8], this is still a doubleing of the peak dose at the end of the antiproton particle track, compared to protons. The loss of the primary beam due to in-flight nuclear reactions is expected to be slighly more than protons, but still less than that of carbon ions [9]. One of the anticipated advantages of the antiproton beam modality compared to protons, Thus, when comparing to protons, the antiproton depth dose curve will look similar to the depth dose curve of protons, but with additional energy deposited in the Bragg-peak from the antiproton annihilation. Antiprotons travel have a slighly longer range than protons, due to the Barkas effect. This effect becomes significant at energies below 300 keV, and will shift the peak no more than $\sim 1\ \mu m$ downstream. The Barkas effect was experimentally veryfied by [10].

Since 2002 the AD-4/ACE collaboration has worked on assesing the dosimetric and radiobiological properties of beams of antiprotons [11–15]. In radiotherapy, where increases of 10 to 20% in the target dose are considered important while sparing the strain on the normal tissue, this could provide a significant enhancement of the therapeutic ratio. [OJ: does a reference exist for this?]

The biological effect of the antiproton beam differs from the depth dose deposition, as the annihilation process yields fragments with a higher Linear Energy Transfer (LET). This means an increased relative biological effectiveness (RBE) in the peak region relative to the plateau region. The biological effect of an antiproton beam was for the first time measured by Holzscheiter et al. [13]. However the RBE in the peak was not measured, as the dosimetry in this region was complicated by both the mixed particle spectrum and the pulsed form of the antiproton beam. Dosimetry with Alanine, Thermoluminescent devices and radiochromic films were tried out, but these suffer from the LET dependence of the response. Calorimetric measurements were considered as too cumbersome. Ionisation chamber measurements were initially believed to be complicated due to the pulsed structure of the antiproton decelerator (AD) antiproton beam at CERN. Later it was realized that Boag's theorem as described in [16] could be applied. Shortly, Boag's theorem is determining the amount of volume recombination by measuring collected charge at two different voltages of the ionization chamber.

2 Experimental Method

The antiproton decelerator at CERN is setup to provide a 502 MeV/c (∼125.85 MeV) antiproton beam. Every 90 seconds a spill of roughly $3 \cdot 10^7$ antiprotons is ejected within 300 ns. The momentum spread of the beam was $\Delta p/p = 10^{-3}$, and the divergence is in the order of 5 mrad. The FWHM of the beam was slightly ellipsoid, being about 1 cm in one axis, and 0.9 cm along the other axis. The beam exited via a thin titanium window and was collimated to 1 cm diameter.

The target phantom is a water tank build of PMMA material according to IAEA and ICRU standards for proton therapy [17, 18]. We used two ionization chambers of the Advanced Roos type chambers from PTW Freiburg. These have graphite electrodes and an active diameter of 39,6 mm. The ionization

chambers are calibrated with ^{60}Co gamma-rays at +400 V towards a reference ionization chamber using the in-house gammatron at the DKFZ. The reference chamber is a PTW Roos ionization chamber M34001 and is calibrated at PTW, being a SSDL secondary standard dosimeter laboratory.

At the antiproton beam line at CERN, one ionization chamber is attached before the entrance window to the water phantom. This chamber is solely used for normalization of the shot to shot fluctuations of the antiproton beam. The second chamber is attached to a calliper which provides submillimeter precision readings of the ionization chamber position. The collected charge is read out with a UNIDOS electrometer.

At each caliper position, data from each shot of antiprotons were recorded. The fixed ionization chamber at the entrance window is kept at +400 V at all times. With the ionization chamber mounted on the water phantom we usually record 4-8 shots at +400 V and 4 shots at +300 V. The electrometer is read out and reset after each shot. At three caliper positions, the entire voltage range from the UNIDOS electrometer is investigated in 50 V steps.

From the measured charge q_1 and q_2 recorded at $V_1 = 400$ V and $V_2 = 300$, respectively, it is possible to apply Boag's theorem. This is done by solving

$$0 = \frac{q}{V} - \frac{\ln(1+u_1)}{\ln(1+u_1 V)} \tag{1}$$

where $q = q_1/q_2$ and $V = V_1/V_2$. Equation 1 is derived from equation 9 in reference [16]. u_1 is related to the collection efficiency f_1 in such a way that:

$$f_1 = \frac{1}{u_1}\ln(1+u_1) \tag{2}$$

In practice, a program was written, which uses the root finding algorithm provided by the Gnu Scientific Library [19]. As a input parameter the measured charges at two voltages are needed. The program then outputs the collection efficiency f_1.

At some caliper positions, we only measure charge at one voltage setting (400 V). Here the charge collection efficiency is interpolated. Beyond the annihilation peak the acquired charge was small and equation 1 has no solution due to statistical fluctuations, and instead the correction efficiency is extrapolated.

The absolute dose D_Q of the antiproton beam quality Q can then be found using the Boag's corrected collected charge $M_{Q,B}$:

$$D_Q = M_{Q,B} N_{Q_0} k_{Q,Q_0} \tag{3}$$

where N_{Q_0} is the ^{60}Co calibration factor. k_{Q,Q_0} is the chamber specific correction factor, but here it was set to 1. For proton beams this factor is expected to be similar to that of the Roos chamber which according to [17] is expected to lie between 1.001 and 1.008.

3 Monte Carlo Calculations

For comparison calculations, both FLUKA v. 2006.3 and SHIELD-HIT v2.2 are used. The geometry applied in FLUKA and SHIELD-HIT consist simply of a 502 MeV/c antiproton beam hitting a 20x20x20 cm water tank. The Gaussian

beam was set to have a FWHM of 1.0 cm and 0.9 cm along x and y axis. In FLUKA the statistics are 150.000 particles. In SHIELD-HIT 100.000 primary particles are simulated.

The scoring region is a stack of discs placed along the beam axis. Each disk is 1 mm thick and a has a diameter of 39,6 mm, matching the effective diameter of the ionization chamber. Since the FWHM of the beam is only in the order of 1 cm, practically all antiprotons are contained in the active scoring region.

For comparison with protons, the FLUKA calculation was repeated using a 5x5 cm square field of antiprotons, maintaining the other beam parameters. The average dose is scored along the beam axis using flat discs with radius 0.5 cm and a thickness of 0.25 mm. Here 300.000 particles are simulated.

4 Results

The measured depth dose curve compared with SHIELD-HIT and FLUKA are shown in figures 1 and 2, respectively. The charge correction efficiency which was applied is shown in figure 3.

The results are here plateau normalized at a depth of 60 mm in order for better showing the deviations in the form of the depth dose curve. The SHIELD-HIT calculations show a deviation of almost 20% in the peak region, whereas FLUKA seem to match the measured depth dose curve very well.

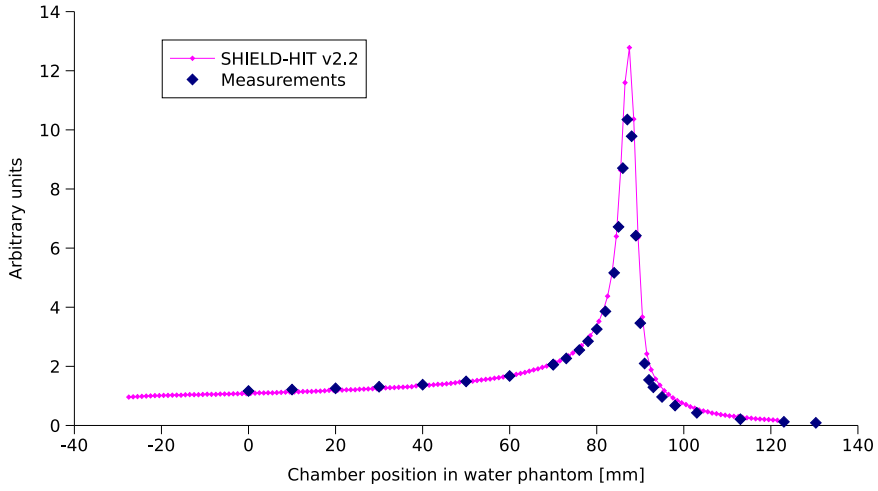

Figure 1: SHIELD-HIT v.2.2 results compared with CERN measurements.

In terms of absolute measurements, our measurements indicated higher doses than calculated with SHIELD-HIT or FLUKA. For each antiproton we measure on average 0,64 ± 0,03 MeV/g deposited dose in the first ionization chamber. Here we assume the same 2% correction from Boag's theorem, as calculated in the second ionization chamber located at position "0 cm". The "0 cm" position corresponds to $\sim 2,8$ cm of water equivalent material (from the ionization

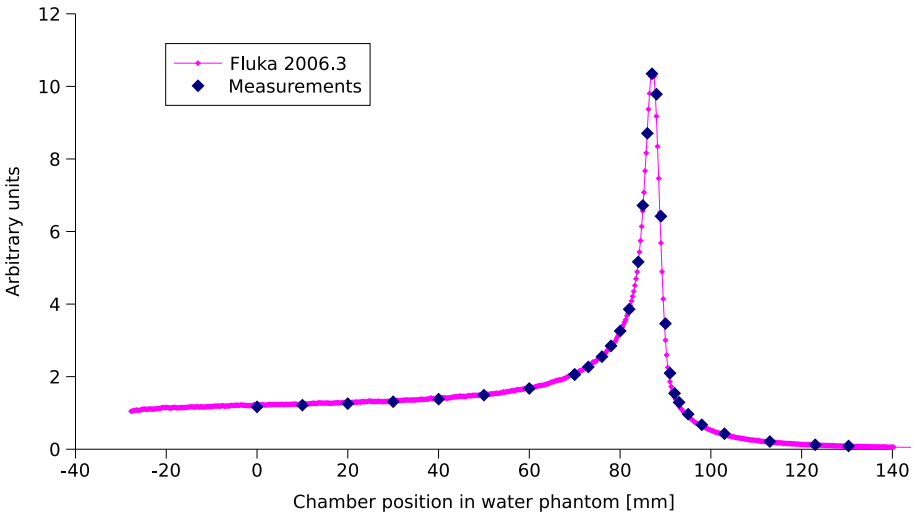

Figure 2: FLUKA 2006.3 results compared with CERN measurements.

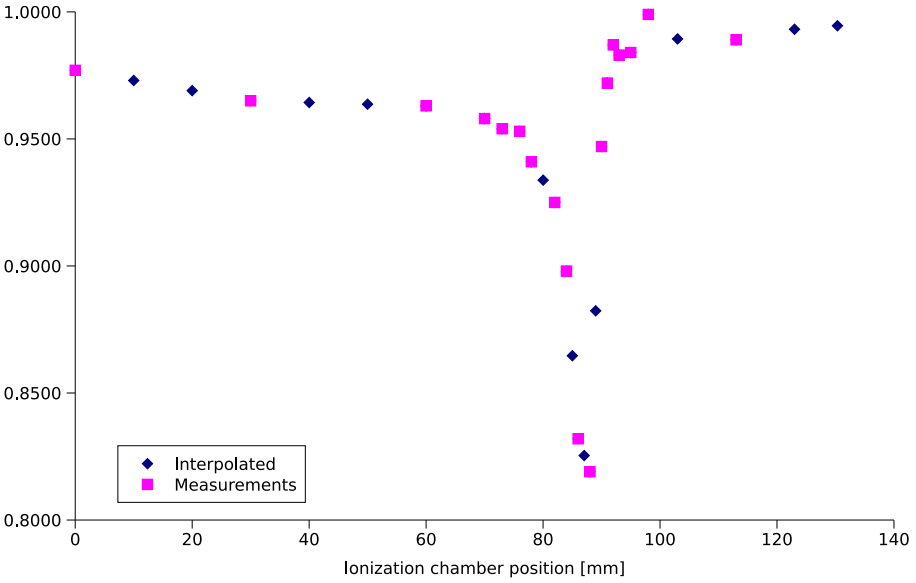

Figure 3: Calculated charge collection efficiency.

chamber thickness and entry window), and was used as a reference point for all measurements.

For the second ionization chamber we see 0,72 ± 0,01 MeV/g of deposited dose in the "0 cm" position, and 1,04 ± 0,02 MeV/g at the "60 cm" position. In table 1 below we compare these values to the those calculated by SHIELD-HIT and FLUKA. The errors stated here are 1σ standard deviations.

	SHIELD-HIT [MeV/g]	FLUKA [MeV/g]	Measurements [MeV/g]
Entry chamber	0,54	0,60	0,64 ± 0,03
Chamber @ "0 cm"	0,59	0,68	0,72 ± 0,01
Chamber @ "60 cm"	0,93	0,95	1,04 ± 0,02

Table 1: Absolute comparison of deposited dose.

A field of antiprotons compared to that of protons is shown in figure 4.

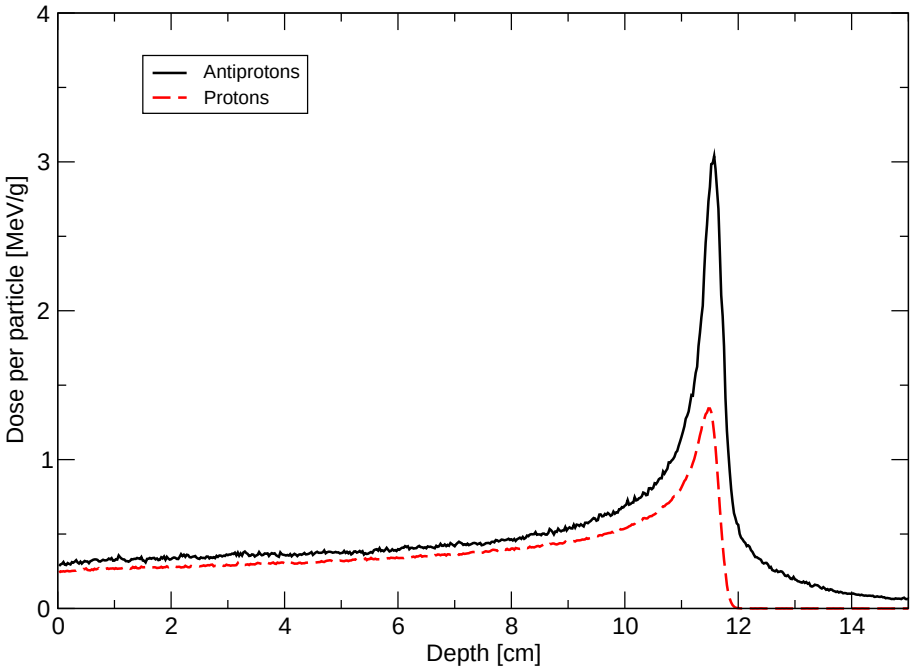

Figure 4: Comparison of depth dose curves from a pristine antiproton beam with a similar proton beam.

5 Discussion

We found excellent agreement between ionization chamber and FLUKA data for relative dose and reasonable agreement in the plateau regions for absolute dose (Error < 6-9%). The origin of the systematic deviation is not clear, but may be possibly be attributed to two sources: First, the Advanced Roos chamber calibration was calibrated towards another ionization chamber which has an

uncertainty of ±4%. Second, the calibration of the beam pickup is good to ±1%.

After verification of FLUKA, this will possibly allow us to extract RBE values from the measurements presented in [13] and future measurements carried out at CERN.

In addition, this will give more credit to the proton - antiproton comparison presented in figure 4. Here we used a broad beam shape in order to more closely match a clinical situation. In principle this beam could be made passively or actively to cover the entire 5x5 cm area. Scoring the central dose region, several features can be observed. In the entry region, a slight elevation of the dose level is seen as compared to protons, arising antiprotons annihilating in-flight. The peak region itself is augmented with over 220% as compared with the proton Bragg-peak, at iso-fluence.

Finally, the different results from SHIELD-HIT is most likely related to different in-flight annihilation cross-sections. The amount of in-flight annihilation cross sections is discussed in [9].

[insert philosophical discussion about antiprotons here]

6 Conclusion

Simulations with FLUKA 2006.3 are in excelent agreement with our relative measurements. In terms of absolute dose, our measurements are 6-9% higher than the FLUKA calculations, but this may be attributed to a beam pickup calibration. SHIELD-HIT v.2.2 overestimated the peak - plateau ratio, which is attributed to the internally used annihilation cross sections.

[insert short conclusion of philosophical disccusion here]

7 Acknowledgements

NB thanks the Danish Cancer Society for supporting this project with a grant. We thank Frank Fabian for assisting at the experiments, and DKFZ for providing the ionization chambers and electrometers.

References

[1] L. Gray and T. E. Kalogeropoulos. Possible biomedical applications of antiproton beams: Focused radiation transfer. *Radiation Research*, pages 246–252, 1984.

[2] M. Inokuti. Interactions of antiprotons with atoms and molecules. *Nucl. Tracks. Radiat. Meas.*, 16(2/3):115–123, 1989.

[3] J. Cugnon, S. Wycech, J. Jastrzębski, and P. Lubiński. Geometrical effects in antiproton annihilation on nuclei. *Physical review C*, 63:027301, 2001.

[4] W. Markiel, H. Daniel, T. von Egidy, F. J. Hartmann, P. Hofmann, W. Kanert, H. S. Plendl, K. Ziock, R. Marshall, H. Machner, G. Riepe, and J. J. Riedy. Emission of helium ions after antiproton annihiliation in nuclei. *Nuclear Physics*, A485:445–460, 1988.

The Antiproton Depth Dose Curve Measured with Alanine Detectors

Niels Bassler[a,b], Johnny W. Hansen[c], Hugo Palmans[d], Michael Holzscheiter[e], Sandra Kovacevic[f] and the AD4/ACE Collaboration[€]

July 5, 2007

a Department of Experimental Clinical Oncology, Aarhus University Hospital, Aarhus, Denmark
b Deutsches Krebsforschungszentrum, Heidelberg, Germany
c Emeritus, formerly Vejle Hospital, Vejle, Denmark.
d National Physical Laboratory, Teddington, Middlesex, UK
e University of New Mexico, Albuquerque, NM, USA
f University of Montenegro, Podgorica, Montenegro

€Michael H. Holzscheiter1, Niels Bassler2,3, Jan Alsner2, Gerd Beyer4, John J. DeMarco5, Michael Doser6, Dragan Hajdukovic7, Oliver Hartley4, Keisuke S. Iwamoto5, Oliver Jäkel3, Helge V. Knudsen8, Sandra Kovacevic7, Søren Pape Møller8, Jens Overgaard2, Jørgen B. Petersen2, Osman Ratib4, Timothy D. Solberg9, Sanja Vranjes10, Bradly G. Wouters11.
1 University of New Mexico, Albuquerque, NM, USA
2 Dept. of Medical Physics and Experimental Clinical Oncology, Aarhus University Hospital, Aarhus, Denmark
3 Deutsches Krebsforschungszentrum, Heidelberg, Germany
4 Hospital Universitaire de Geneve, Geneva, Switzerland
5 David Geffen School of Medicine, UCLA, Los Angeles,CA, USA
6 CERN, Geneva, Switzerland
7 University of Montenegro, Podgorica, Montenegro
8 Dept. of Physics & Astronomy and ISA, University of Aarhus, Aarhus, Denmark
9 University of Nebraska Medical Center, Omaha, NE, USA
10 VINCA Institute for Nuclear Sciences, Belgrade, Serbia
11 University of Maastricht, Res. Institute Growth and Development, The Netherlands.

Running Title: Antiproton Dosimetry with Alanine

Corresponding author:

Niels Bassler, PhD n.bassler@dkfz.de

DKFZ – E040
Im Neuenheimer Feld 280
D-69120 Heidelberg
Germany

Phone : +49 (0) 6221 422596

1 Abstract

In this paper we report on the measurement of the antiproton depth dose curve, with alanine detectors. The results are compared with simulations using the particle energy spectrum calculated by FLUKA, and using the track structure model of Hansen et Olsen for conversion of calculated dose into response. A good agreement was observed between the measured and calculated relative effectiveness although a slight underestimation of the calculated values in the
Bragg peak remains unexplained. The model prediction of response of alanine towards heavy charged particles encourages future use of the alanine detectors for dosimetry of mixed radiation fields.

2 Introduction

Antiproton radiotherapy was first suggested by Gray and Kalogeropoulos in 1984 [1]. One of the anticipated advantages of antiprotons compared to protons, is the additional energy deposited at the Bragg-peak from the antiproton annihilation. Sullivan suggested in [2] that the additional local energy deposited by the annihilation products may roughly be about 30 MeV. Even though this value sounds low compared with the total of 1.88 GeV released by the annihilation, this still results in a substantial augmentation of the peak dose at the end of the particle track.

To interpret a measured response of a biological system exposed to a beam of hadrons in terms of dose deposition, a prediction of the Relative Biological Effectiveness (RBE) for the particular beam of particles is necessary. Similarly, for a radiation detector the relative effectiveness (RE) is relating the observed detector response with dose deposition. The observed response of a detector is here expressed in terms of the dose R, which is the dose as read from the gamma
response curve. This term will exclusively be used here to express response. For the dose D_{ion} deposited by ions, we have

$$R_{ion} = RE \cdot D_{ion} \qquad (1)$$

Thus, R_{ion} is the response of a detector exposed to ion beams expressed in terms of the dose by _-rays, neccessary to produce equal response. Here, “ion” means any particle with $Z \geq 1$. Note, that often the term Heavy Charged Particles (HCPs) is used, referring to particles with $Z > 1$.
For a given biological system and chosen endpoint, RBE is a function of the target parameters, atomic number and velocity of the bombarding particle, why the biological effect per unit dose changes with the penetration depth of the particle. Thus the RBE in the plateau region is different from that in the Bragg-peak. The difference of plateau and peak RBE increases significantly with atomic number of the projectile. For protons one generally assumes an RBE close to unity for the entire penetration, even though an increase of RBE beyond this value has been observed for the distal edge of the Bragg peak [3, 4].

For HCPs the increase of RBE with depth becomes more pronounced and also shifts towards the entrance to the target with increasing atomic number. For antiprotons compared to protons of the same energy, the difference in RBE is further enhanced in the peak region, due to the annihilation process which also yields fragments with $Z > 1$. In the plateau region, antiprotons are expected to behave similar as protons.

Attempts to measure the RBE directly in the peak region so far have failed, since dosimetry of the antiproton depth dose curve is problematic due to the unknown dosimeter response [5–7]. Ionization chambers behave non-linear too, due to volume recombination [8] arising from the pulsed nature of the antiproton beam available at CERN. Measurements using Boag’s theorem [9] correcting for recombination effects have been performed and a publication on this is in preparation. Calorimetry is the most direct way to measure absorbed dose according to its definition. However, calorimeters are cumbersome to use and are not easily applicable in a low-frequency pulsed beam such as CERN’s antiproton beam. Other detectors we have applied in the antiproton beam are Thermoluminescent Devices (LiF based) and radiochromic films [10]. This paper, however, will concentrate on the results achieved with alanine detectors.

The response of alanine detectors to HCPs was investigated by Hansen and Olsen in the 80's [11, 12]. A model explaining the behaviour based upon the Butts and Katz track structure idea [13, 14] was conceived [15]. This model has had some success in predicting the RE of alanine detectors, including fading effects: most solid state radiation detectors show a post-irradiation time dependent change in response when exposed to saturation doses, a phenomenon being of importance in the evaluation of dose-response for detectors exposed to beams of HCPs. Though alanine has been reported to have a high time stability of radiation induced response to gamma rays of doses less than 10^4 Gy, considerable decay has been observed after low average doses from heavy charged particles. The amount of decay has been found as well to be dependent on the ion parameters [16], more precisely, on the radial dose distribution around the particle track. Predictions based on the model of track structure have shown to conform to experimental data [12]. Then due to the higher atomic number annihilation fragments in the Bragg peak of antiprotons the fading processes will be more pronounced and should from a theoretical point of view be taken into account when comparing the radiation effect in the Bragg peak with that
of protons.

The decay in alanine is dominant within the first 100 to 200 hours after exposure to HCPs, and the rate of decay is different for pellets positioned in the plateau compared to those in the Bragg-peak [16]. E.g. a 250 MeV/u carbon ion fades 1.6% after 1900 hours. At 1 MeV the fading approaches 5 %. When irradiated with 250 and 1 MeV protons the response fades 1.6% and 2.3% after 1900 hours.

Here we shall apply the track structure model on a mixed particle energy spectrum simulated by FLUKA, in order to calculate the RE and then the expected response of alanine pellets based on the measured gamma-ray dose-response curve. The predicted response as a function of penetration depth is compared to that measured from a stack of alanine pellets exposed to a beam of antiprotons.

3 Experimental Methods

Two stacks of alanine pellets were irradiated with antiprotons. The pellets in stack #1 consisted of finely grained crystalline alanine powder (Merck) 95% by weight mixed with 5% by weight polyvinyl-pyrrolidone (Polyvidone, Merck) as the binding agent and were manufactured by J.W. Hansen. The pellets had an outer diameter of 4.5 mm, a thickness of 2 mm, and a density of 1.21 g cm^{-3}. Details about the dosimeter pellets have been published [15]. In this stack seven pellets were placed in the plateau, and 18 pellets were placed around the annihilation peak.
Stack #2 consisted of alanine pellets which were produced by NPL and constituted of 90% by weight L-_-alanine and 10% high melting point paraffin wax. The diameter of the pellets was 5 mm and the thickness was either 2.2 mm or 0.44 mm (average values for the entire batch). The average density was 1.24 g cm^{-3}. The stack was assembled from eleven 2.2 mm pellets, six 0.44 mm pellets and five 2.2 mm pellets, arranged in a 5.2 mm cylindrical hole in a PMMA phantom. A build-up plate of 81.8 mm polystyrene was used in order to position the Bragg peak around the position of the thin pellets.

The Antiproton Decelerator (AD) at CERN provided a 502 MeV/c (~126 MeV) antiproton beam. Every 90 seconds a spill consisting of roughly $3 \cdot 10^7$ antiprotons was ejected within 300 ns. The momentum spread of the beam was $\_p/p = 10^{-3}$, and the divergence in the order of 5 mrad. The absolute number of particles extracted from the AD was determined by a fast current transformer mounted downstream of the extraction septum in the DEM beam line, feeding our experimental set-up. Earlier studies showed that this number may have a tendency to overestimate the fluence at the target by 10 - 20%. This may be due to calibration errors and/or to losses in the final stretches of the beam line leading up to our set-up. The beam exited the accelerator vacuum via a thin titanium window and was collimated to 1 cm diameter.

The alignment of the two stacks was verified with two radiochromic films (GAFChromic) which were inserted along the beam. The FWHM of the beam when irradiating stack #2 was almost circular with a FWHM of 0.9 - 1.0 cm. The beam which was used for stack #1 had a more ellipsoid form of roughly 0.6 - 1.0 cm FWHM. Stack #1 was read out by the Radiation Research Department at the Risø National

Laboratory in Denmark, using a Bruker EMS 104 EPR alanine readout device. Stack #1 was read out several times at increasing time intervals, in order to detect any fading effects, as reported in [16]. At each readout, the pellet was measured at zero and 90° rotation and a mean signal strength was obtained. Stack #2 was read out at the National Physics Laboratory (NPL) in the UK using the standard procedures for NPL's radiotherapy level alanine dosimetry service [17]. The spectrometer was a Bruker ESX and a standard Bruker ST4102 rectangular cavity. The acquisition time was 120 s consisting of six 20 s scans with 90° rotation of the pellet between the third and fourth scan. The pellets were introduced in the spectrometer using an automated loading system with a specially constructed sample holder to provide highly accurate positioning [18].

4 Monte Carlo Calculations

FLUKA [19, 20] version 2006.3 was used for calculating the antiproton particle transport through the medium, and the distribution of secondaries in each alanine pellet. The beam profiles measured with the radiochromic films was used as input parameter for FLUKA for stack #1 and stack #2. For example for stack #1 a little misalignment of 2 mm and a rotation of the phantom of a few degrees was applied. 100.000 particles were used for the statistics. The dose D from all particles (including contribution from gamma-rays) was scored in every pellet position. In addition, the track length fluence-energy spectrum _[E_j,Z_i] for pions, protons, deuterium, tritons, He-3 and He-4 was recorded for each pellet using the USRTRK card in FLUKA. _[E_j,Z_i] is thus a matrix divided in particle types Z_i and energy bins with the mean energy E_j. Since π^+ and π^- both have unity charge, charged pions are treated as protons with A = 0.15 amu. π^0 particles are neglected as they decay instantaneously into gamma rays. Antiprotons are treated as protons.

The track length dose D_{TL} can be derived from _[E_j ,Z_i] as:

$$D_{TL} = \sum_{i=1}^{Z_{proj}} \sum_{j=1}^{E_{bin}} \Phi\left[E_j, Z_i\right] \frac{1}{\rho} \frac{dE}{dx}(E_{j,} Z_i) \quad (2)$$

where $\frac{1}{\rho}\frac{dE}{dx}(E_{j,} Z_i)$ is the mass stopping power for particle Z_i at energy E_j .

The stopping power is evaluated at the center of the energy bin using the PSTAR and ASTAR routines by Berger et al. [21]. MSTAR (by Paul and Shinner [22,23]) support is included in the data reduction program, but was not used, as nuclei with Z > 2 were ignored. The dose D_{TL} calculated by the track length fluence, is lower than the FLUKA dose D, since photons and particles heavier than He-4 are not included in the D_{TL} calculation. The difference is usually
about 1-2% in the plateau region and about 7% in the pellet(s) covering the peak region.

From the track length fluence matrix _[E_j,Z_i] the relative effectiveness of each particle-energy entry is looked up in a table. This RE table is generated using the model by Hansen and Olsen for infinitesimal thin detectors. By summing all individual detector responses $R_{ion}(E_j ,Z_i) = RE(E_j,Z_i)D(E_j,Z_i)$ for each energy bin E_j and particle type Z_i, a total dose weighted average relative
effectiveness RE of the particle spectrum is found for this particular pellet:

$$\overline{RE} = D_{TL}^{-1} \sum_{i=1}^{Z_{proj}} \sum_{j=1}^{E_{bin}} RE(E_{j,} Z_i) \Phi\left[E_j, Z_i\right] \frac{1}{\rho} \frac{dE}{dx}(E_{j,} Z_i) \quad (3)$$

The calculated RE multiplied with the total dose D (now including all fragments) for the pellet scored by FLUKA in combination with the measured _-ray dose-response curve gives the predicted response of the pellet. In terms of response equivalent _-ray dose R, we have:

$$R_{ion}(D) = \overline{RE} \cdot D \quad (4)$$

.

5 Results

In the figures 1 and 2 below, the total measured response of the alanine pellets as a function of penetration depth is plotted together with the response calculations and the predicted dose for stack #1 and #2 respectively. Fading effects were included in these calculations. The response is expressed in terms of response equivalent gamma dose.

All measurements are absolute, as the total number of antiprotons were measured upstream the beam with the beam current transformer. This may introduce a systematic error, as some of the beam may be lost on the way from the transformer to the experimental setup, as mentioned earlier. For stack #1 in figure 1 the measurements have been shifted by 1.5 mm along the beam axis, in order to match the peaks (see below). The fading of the alanine tablets was investigated with alanine stack #1. Unfortunately the ESR-spectrometer for these readings turned out to be very unstable resulting in unreliable measurements for which fading could not be determined with a sufficient accuracy. From calculated predictions we expect to find a difference of approx. 1% in fading between dosimeters positioned at the plateau and in the peak. Most of this fading in response is considered to take place within 200 hours after irradiation. Here we applied 800 hours for the stack #1 and 1900 hours for stack #2, but the fading effects are too small to be observable.

[figure1: `johnny_pub.eps`]
Figure 1: Stack #1 results. The dotted line shows the dose for each pellet as it is calculated by FLUKA. The calculated dose multiplied with the calculated relative effectiveness is plotted as a solid line, and should ideally match the measurements marked as unconnected squares. Measured response is translated to dose using the _-ray dose-response curve.

[figure2: `hugo_pub.eps`]
Figure 2: Results for stack #2 plotted in the same fashion as figure 1. The measurements were not shifted along the x-axis, though.

Using equation 3 the calculated relative effectiveness as a function of the particle penetration depth for stack #2 is shown in figure 3.

[figure3: `eta.eps`]
Figure 3: Calculated relative effectiveness for stack #2. The relative effectiveness drops off in the peak region due to the the slowing down of antiprotons and the annihilation products with higher LET.

6 Discussion

One of the major differences between stack #1 and #2, was the fitting of the pellet diameter to the ∅5 mm hole drilled into the phantom. The stack #1 leaved a gap in between the pellet and the cavity wall whereas the stack #2 pellets did fit the hole exactly. The presence of this gap enables some antiprotons to tunnel past the pellets. Furthermore, the pellets in stack #1 did not have a
perfect cylindrical form, but had a little edge at the rim of the outer diameter. This will increase the amount of range straggling of the antiproton beam, thus widening the peak, and localizing it further downstream the beam axis. This may possibly explain the shift of 1.5 mm downstream from the predicted position of the measured peak. This effect is thought to be much less pronounced for stack #2, as these pellets had perfect cylindrical form which closely matched
the phantom cavity.

Another difference between both stacks was the density matching of the pellets and the surrounding phantom. For stack #1 the alanine pellets had 1.21 g cm^{-3} and were surrounded by polystyrene with 1.04 g cm^{-3}. For stack #2 the 1.24 g cm^{-3} pellets were surrounded by a PMMA phantom with a density of 1.19 g cm^{-3}. This effect is responsible for the difference in the shape of the tail since antiprotons can penetrate

deeper in the surrounding phantom as in the alanine stack and their annihilation can contribute dose beyond the Bragg peak.

Both stacks provide absolute dose measurements. Since the plateau region of the stack #2 fits the calculations very well, the systematic effect of a possible overestimate of the recorded particle fluence due to the upstream position of the beam current transformer seems to be minor. Absolute dose measurements for stack #1 are more problematic, since the alanine readout device had a tendency to drift.

The RE is fairly close to unity in the plateau region, and drops down to about 0.8 in the peak region. The reason for this rather slight change in RE is due to the low atomic number of the antiproton itself but also due to the resulting mixed field of relative light nuclei from the antiproton annihilation. According to Polster et al. [24] the field in the peak region consists mostly of relative light nuclei of high energy, which is also what we see in our FLUKA calculations. Those fragments have fairly high REs due to the high energies of the secondary particles, compared to that of stopping antiprotons.

The nature of the slight overestimation of the calculated dose maximum in the annihilation peak is rather unclear. Several possible explanations exist:

- the RE model has shown [12] to be only partially correct for HCP-energies below 2 MeV/u
- errors in the geometry used as input parameter for the FLUKA calculations
- omission of $Z > 2$ particles in D_{TL} and the RE calculation in equations 2 and 3
- limitation of the inherent model in the FLUKA code to predict the annihilation peak accurately

On the experimental side a source of error may be the fact that the pellets consists of grains in a matrix whereas the Monte Carlo simulations assume a homogeneous mixture. Finally, the local shape of the annihilation peak is very sensitive to volume averaging effects, which may not be reproduced accurately in the Monte Carlo simulation. In the end, we can state that alanine together with model calculations of RE is a perfect dosimeter in mixed radiation fields as former shown for neutrons [25].

Models based on track structure theory by Katz, and derivatives of the Local Effect Model such as ECLaT [26] for Thermoluminescent Devices (TLDs), rely on predicting the response of a detector from the gamma-response curve which is convoluted with the radial dose distribution of a track in order to achieve the relative effectiveness of the HCP radiation in question.

Here, the response calculations are further simplified since interactions between two or multiple tracks were not considered. The inclusion of track interactions in the RE-calculation would lead to a lower predicted RE and thus to less calculated response. Track interactions are most likely to happen at high fluences where the mean track distance $\sqrt{\varphi^{-1}}$ becomes similar to that part of the track radius in which ”cross-overs” would lead to saturation response. The neglect of track interactions in the calculation of effectiveness is most likely possible due to the high saturation dose of alanine. The region of saturation in a single particle track is smaller in a detector with a high saturation level, i.e. low radiation sensitivity, than that of a detector with a low saturation level, i.e. high radiation sensitivity. Therefore the effect of overlapping tracks is expected to be low for the alanine detector.

7 Conclusion

In this paper we have used alanine detectors for the dosimetry of the mixed particle field arising from antiproton annihilation. We believe that Alanine is very suitable for this kind of dosimetry. The antiproton depth dose curve was measured with alanine pellets. The results could be reproduced using the relative effectiveness calculated with Hansen’s and Olsen’s track structure model used in conjunction with doses and particle spectra calculated with FLUKA. The alanine detector is a good detector for characterizing the mixed radiation field from antiproton annihilation. This detector could also be applied for dosimetry of medical heavy ion beams and possibly in mixed radiation fields found in space.

8 Acknowledgements

We thank Peter Sharpe and Clare Gouldstone from NPL and Jakob Helt from Risø for reading out the alanine dosimeters. The Danish Cancer Society supported this project with a grant.

References

[1] L. Gray and T. E. Kalogeropoulos. Possible biomedical applications of antiproton beams: Focused radiation transfer. Radiation Research, 97:246–252, 1984.

[2] A. H. Sullivan. A measurement of the local energy deposition by antiprotons coming to rest in tissue-like material. Phys. Med. Biol., 30(12):1297–1303, 1985.

[3] Jay S. Loeffler, A. R. Smith, and H. D. Suit. The potential role of proton beams in radiation oncology. Seminars in Oncology, 24(6):686–695, 1997.

[4] B. G. Wouters, G. K. Y. Lam, U. Oelfke, K. Gardey, R. E. Durand, and L. D. Skarsgard. Measurements of relative biological effectiveness of the 70 MeV proton beam at TRIUMF using chinese hamster V79 cells and the high-precision cell sorter assay. Radiation Research, 146(2):159–170, 1996.

[5] Michael H. Holzscheiter, Nzhde Agazarayan, Niels Bassler, Gern Beyer, John J. DeMarco, Michael Doser, Toshiyasu Ichioka, Keisuke S. Iwamoto, Helge V. Knudsen, and Bradly G. Wouters. Biological effectiveness of antiproton annihilation. NIM B, 221:210–214, 2004.

[6] Carl Maggiore, Nzhde Agazarayan, Niels Bassler, Ewart Blackmore, Gerd Beyer, John J. DeMarco, Michael Doser, Charles R. Gruhn, Michael H. Holzscheiter and Bradly G.Wouters. Biological effectiveness of antiproton annihilation. NIM B, 214:181–185, 2004.

[7] Michael H. Holzscheiter, Niels Bassler, Nzhde Agazaryan, Gerd Beyer, Ewart Blackmore, John J. DeMarco, Michael Doser, Ralph E. Durand, Oliver Hartley and Bradly G. Wouters. The biological effectiveness of antiproton irradiation. Radiotherapy and Oncology, 81(3):233–242, December 2006.

[8] Frank H. Attix. Introduction to Radiological Physics and Radiation Dosimetry. John Wiley & Sons, 1986.

[9] J. W. Boag and J. Currant. Current collection and ionic recombination in small cylindrical ionization chambers exposed to pulsed radiation. British Journal of Radiology, 53:471–478, 1980.

[10] Niels Bassler. Experimental Studies Relevant for Antiproton Cancer Therapy. PhD thesis, Aarhus University, May 2006.

[11] J. W. Hansen and K. J. Olsen. Theoretical and experimental radiation effectiveness of the free radical dosimeter alanine to irradiation with heavy charged particles. Radiation Research, 104:15–27, 1985.

[12] K. J. Olsen and J. W. Hansen. The response of the alanine dosemeter to low energy protons and high energy heavy charged particles. Radiation Protection Dosimetry, 31(1/4):81–84, 1990.

[13] J. J. Butts and Robert Katz. Theory of RBE for heavy ion bombardment of dry enzymes and viruses. Radiation Research, 30:855–871, 1967.

[14] R. Katz, S. C. Sharma, and M. Homayoonfar. The structure of particle tracks. In F. H. Attix, editor, Topics of Radiation Dosimetry, volume Suppl. 1, pages 317–383. New York Academic Press, 1972.

[15] J. W. Hansen. Experimental Investigation of the Suitability of the Track Structure Theory in Describing the Relative Effectiveness of High-LET Irradiation of Physical Radiation Detectors. PhD thesis, Risø National Laboratory, DK-4000 Roskilde, 1984. Risø-R-507.

[16] J.W. Hansen and K. J. Olsen. Predicting decay in free-radical concentration in L-_-Alanine following high-LET radiation exposures. Appl. Radiat. Isot., 40(10-12):935–939, 1989.

[17] P. H. Sharpe, K. Rajendran, and J. P. Sephton. Progress towards an alanine/ESR therapy level reference dosimetry service at NPL. Appl Radiat Isot., 47(11-12):1171–5, Nov-Dec 1996.

[18] P. Sharpe and J. Sephton. An automated system for the measurement of alanine/EPR dosimeters. Appl Radiat Isot., 52(5):1185–8, May 2000.

[19] A. Fasso', A. Ferrari, J. Ranft, and P. R. Sala. FLUKA: a multi-particle transport code. CERN-2005-10, INFN/TC 05/11, SLAC-R-773.

[20] The physics models of FLUKA: status and recent developments, La Jolla, CA, USA, March 24-28 2003. (paper MOMT005), eConf C0303241 (2003), arXiv:hep-ph/0306267.

[21] M. J. Berger, J. S. Coursey, M. A. Zucker, and J. Chang. Stopping-power and range tables for electrons, protons, and helium ions.
http://physics.nist.gov/PhysRefData/Star/Text/contents.html.

[22] H. Paul and A. Schinner. MSTAR.
http://www.exphys.uni-linz.ac.at/stopping/.

[23] H. Paul and A. Schinner. An empirical approach to the stopping power of solids and gases for ions from $_{3}$Li to $_{18}$Ar. NIM B, 179:299, 2001.

[24] D. Polster, D. Hilscher, H. Rossner, T. von Egidy, F. J. Harmann, J. Hoffmann, W. Schmid, I. A. Pshenichnov, A. S. Iljinov, Ye. S. Golubeva, H. Machner, H. S. Plendl, A. Grouchulska, J. Jastrzebski, W. Kurcewiz, P. Lubinski, J. Eades, and S. Neumaier. Light particle emission induced by stopped antiprotons in nuclei: Energy dissipation and neutron-to-proton ratio. Physical Review C, 51(3):1167–1180, 1995.

[25] H. M. Gerstenberg, J. W. Hansen, J. J. Coyne, and J. Zoetelief. Calculations of the relative effectiveness of alanine for neutrons with energies up to 17.1 MeV. Radiation Protection Dosimetry, 31(1/4):85–89, 1990.

[26] O. B. Geiß, M. Krämer, and G. Kraft. Efficiency of thermoluminescent detectors to heavy charged particles. NIM B, 142:592–598, 1998.

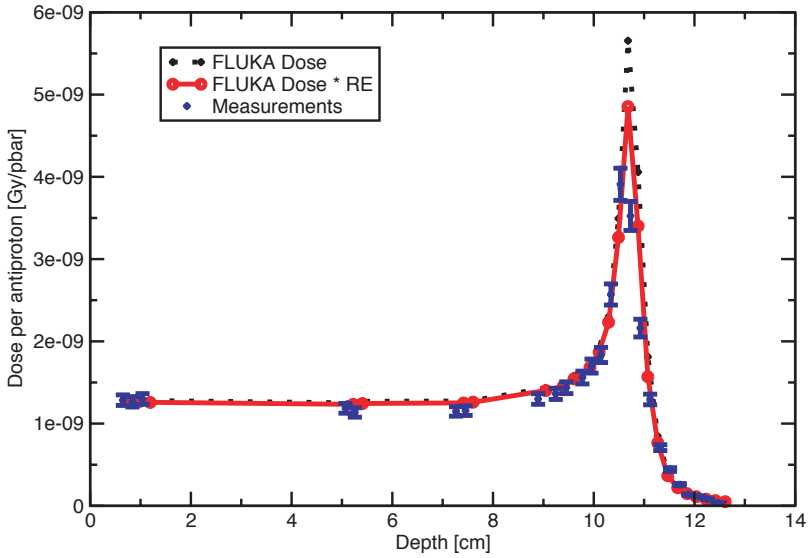

Figure 1

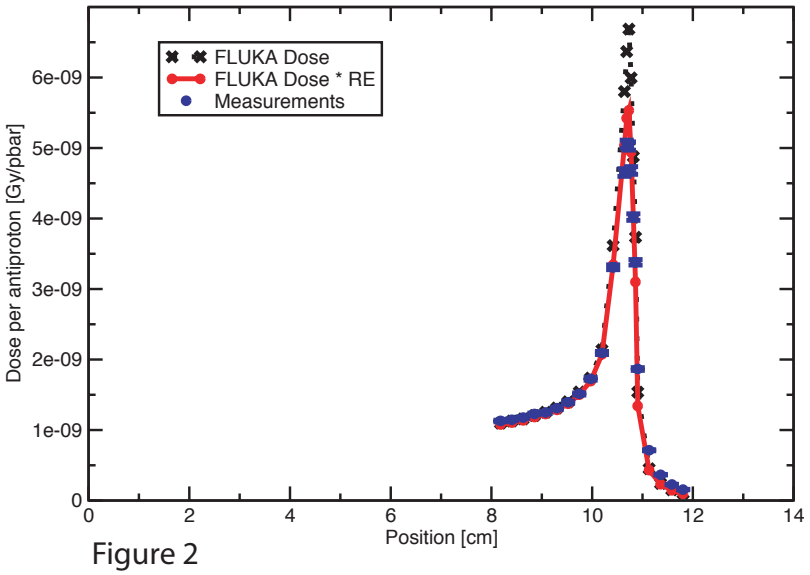

Figure 2

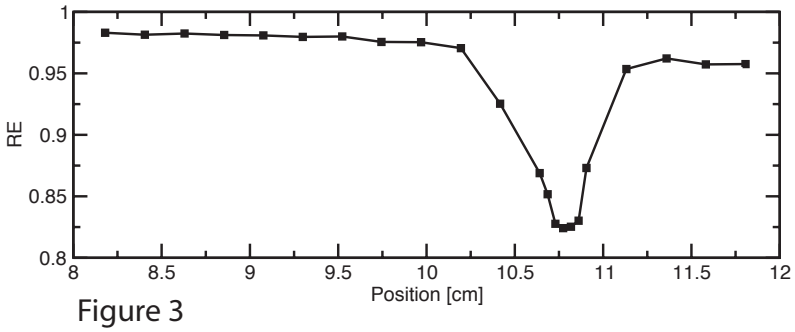

Figure 3